A HIGH-ORDER ACCURATE PARALLEL SOLVER FOR MAXWELL'S EQUATIONS ON OVERLAPPING GRIDS

WILLIAM D. HENSHAW*

Abstract. A scheme for the solution of the time dependent Maxwell's equations on composite overlapping grids is described. The method uses high-order accurate approximations in space and time for Maxwell's equations written as a second-order vector wave equation. High-order accurate symmetric difference approximations to the generalized Laplace operator are constructed for curvilinear component grids. The modified equation approach is used to develop high-order accurate approximations that only use three time levels and have the same time-stepping restriction as the second-order scheme. Discrete boundary conditions for perfect electrical conductors and for material interfaces are developed and analyzed. The implementation is optimized for component grids that are Cartesian, resulting in a fast and efficient method. The solver runs on parallel machines with each component grid distributed across one or more processors. Numerical results in two- and three-dimensions are presented for the the fourth-order accurate version of the method. These results demonstrate the accuracy and efficiency of the approach.

Key words. Maxwell's equations, overlapping grids, high-order accurate, symmetric finite difference

AMS subject classifications. 65M06, 65M12, 78M20

1. Introduction. A numerical scheme is described for the fast and accurate solution of the time dependent Maxwell's equations in complex geometry. Maxwell's equations are solved as a second-order vector wave-equation rather than the more common approach of treating the equations as a first-order system. The governing equations are discretized to high-order accuracy in space and time on domains that are represented with composite overlapping grids. High-order accurate symmetric finite difference discretizations of the generalized Laplace operator are devised for use on curvilinear grids. High-order accurate centered approximations for boundary conditions are developed and analyzed. The three-level time stepping scheme is based on the modified equation approach and achieves high-order accuracy through a Taylor series in time that uses the differential equations to replace time derivatives by space derivatives. The time step restriction, as dictated by stability, is the same as that used with the second-order version of the method. The interface between materials with different electric and magnetic properties is treated using component grids that align with the interface. High-order accurate centered approximations to the interface jump conditions are developed that maintain the full accuracy of the scheme at the interface. The numerical approach presented here is particularly fast and efficient on Cartesian component grids. A typical overlapping grid for a region Ω will consist of body fitted curvilinear grids near the boundaries together with one or more background Cartesian grids covering most of the domain. For sufficiently fine grids, the majority of the grid points will reside on the Cartesian grids. In this case, the efficiency of the scheme approaches that of a single Cartesian grid.

The time dependent Maxwell's equations for linear, isotropic and non-dispersive materials are

$$\partial_t \mathbf{E} = \frac{1}{\epsilon} \nabla \times \mathbf{H} - \frac{1}{\epsilon} \mathbf{J}, \tag{1.1}$$

$$\partial_t \mathbf{H} = -\frac{1}{\mu} \nabla \times \mathbf{E}, \tag{1.2}$$

$$\nabla \cdot (\epsilon \mathbf{E}) = \rho, \quad \nabla \cdot (\mu \mathbf{H}) = 0, \tag{1.3}$$

Here $\mathbf{E} = \mathbf{E}(\mathbf{x}, t)$ is the electric field, $\mathbf{H} = \mathbf{H}(\mathbf{x}, t)$ is the magnetic field, $\rho = \rho(\mathbf{x}, t)$ is the electric charge density, $\mathbf{J} = \mathbf{J}(\mathbf{x}, t)$ is the electric current density, $\epsilon = \epsilon(\mathbf{x})$ is

the electric permittivity, and $\mu = \mu(\mathbf{x})$ is the magnetic permeability. This first-order system for Maxwell's equations can also be written in a second-order form. By taking the time derivatives of (1.2) and (1.1) and using (1.3) it follows that

$$(1.4) \qquad \epsilon\mu \, \partial_t^2 \mathbf{E} = \Delta \mathbf{E} + \nabla\left(\nabla \ln \epsilon \, \cdot \mathbf{E}\right) + \nabla \ln \mu \times \left(\nabla \times \mathbf{E}\right) - \nabla(\frac{1}{\epsilon}\rho) - \mu\partial_t\mathbf{J},$$

$$(1.5) \qquad \epsilon\mu \, \partial_t^2 \mathbf{H} = \Delta \mathbf{H} + \nabla\left(\nabla \ln \mu \, \cdot \mathbf{H}\right) + \nabla \ln \epsilon \times \left(\nabla \times \mathbf{H}\right) + \epsilon\nabla \times (\frac{1}{\epsilon}\mathbf{J}).$$

It is evident that the equations for the electric and magnetic field are decoupled with each satisfying a vector wave equation with lower order terms. In the case of constant μ and ϵ and no charges, $\rho = \mathbf{J} = 0$, the equations simplify to the classical second-order wave equations,

$$(1.6) \qquad\qquad\qquad \partial_t^2 \mathbf{E} = c^2 \, \Delta \mathbf{E}, \qquad \partial_t^2 \mathbf{H} = c^2 \, \Delta \mathbf{H}$$

where $c^2 = 1/(\epsilon\mu)$. There are some advantages to solving the second-order form of the equations rather than the first-order system. One advantage is that in some cases it is only necessary to solve for one of the variables, say $\mathbf{E}$. If the other variable, $\mathbf{H}$ is required, it can be determined by integrating equation (1.2) as an ordinary differential equation with known $\mathbf{E}$. Alternatively, as a post-processing step $\mathbf{H}$ can be computed from an elliptic boundary value problem formed by taking the curl of equation (1.1). Another advantage of the second-order form, which simplifies the implementation on an overlapping grid, is that there is no need to use a staggered grid formulation. Many schemes approximating the first order system (1.2-1.3) rely on a staggered arrangement of the components of $\mathbf{E}$ and $\mathbf{H}$ such as the popular Yee scheme [44] for Cartesian grids. From a numerical point of view, there is an advantage in that the principal part of the spatial operator of the second-order system (1.4) is the Laplace operator Δ, which is a strongly elliptic operator and thus amenable to the discretization through compact difference approximations. The corresponding operator $-\nabla \times \nabla$ for the first order system (1.1-1.2), on the other hand, has a large null space consisting of all functions that are a gradient of a scalar field, and requires more care in discretizing. The development of appropriate boundary conditions is sometimes cited as a disadvantage of solving the second-order form of the equations. The second-order continuous formulation requires additional boundary conditions as discussed in section 2, as well as additional numerical boundary conditions for higher-order accurate discretizations. A primary purpose of this work is to show how to define accurate centered-approximations to the boundary conditions that are based upon compatibility conditions consistent with the governing equations.

There have been a variety of numerical approaches developed for solving the Maxwell's equations in the time-domain and there is extensive literature on the subject including the books by Cohen [4], and Taflove and Hagness [41]. Some references to the different approaches will now be given. One of the most popular approaches is the staggered grid scheme of Yee [44], commonly known as the FDTD (finite-difference time-domain) method. For complex geometry, a *stair-step* approximation to the boundary is often used with the scheme. Improvements to the accuracy of the basic stair-step technique have been considered, by for example, Dey and Mitra [7], Ditkowski, Dridi and Hesthaven [9] and Kreiss and Petersson [27]. The Yee scheme has been extended to curvilinear grids, see for example, Lee, Palendech and Mittra [30] and to unstructured grids such as in the DSI (discrete surface-integral) scheme originally developed by Madsen [32] and extended by Gedney [13]. Finite volume methods have been applied to the solution of Maxwell's equations as discussed for example in Holland [24]. Jurgens and Zingg [26] use high-order finite difference approximations on block-structured grids for the equations written as a first-order system. Schemes based on the finite-element-method (FEM) have been developed to solve Maxwell's equations, see for example, Nedelec [33], Jin [25], and Rodrigue and White [37]. The spectral element method has been used by a variety of authors including Yang, Gottlieb and Hesthaven [43]. High-order spectral penalty-methods and discontinuous Galerkin type approaches have also been successful, see for example, Hesthaven and

Warburton [23]. Use of hybrid grids, part structured and part unstructured, has become increasingly popular. Rylander and Bondeson [38], for example, present a hybrid FEM-FDTD method that retains the symmetry of the discrete operators, even at the interface between the FEM and FDTD methods. Yee, Chen and Chang [45] considered the solution of Maxwell equations on overlapping grids using a second-order accurate method. Driscoll and Fornberg [10, 11] have developed a block pseudo-spectral method for Maxwell's equations on two-dimensional overlapping grids. They solve the equations as a first-order system using a high-order difference method on the Cartesian background grid and a pseudo-spectral method on the boundary fitted curvilinear grids.

2. Governing equations and boundary conditions. The numerical scheme is based upon the solution of the second-order form of Maxwell's equations. To begin with, the material properties $\epsilon(\mathbf{x})$ and $\mu(\mathbf{x})$ are assumed to be constant. The case of multiple materials will be treated in section 7. In three space dimensions, the initial boundary value problem for Maxwell's equations on a domain Ω is given by

$$(2.1) \qquad \partial_t^2 \mathbf{E} = c^2\,\Delta\mathbf{E}, \qquad\qquad \mathbf{x} \in \Omega,$$

$$(2.2) \qquad \mathbf{n} \times \mathbf{E} = 0, \ \ \nabla \cdot \mathbf{E} = 0, \qquad \mathbf{x} \in \partial\Omega_E, \quad \text{(PEC BC's)}$$

$$(2.3) \qquad \mathcal{B}_F(\mathbf{E}) = 0, \ \ \nabla \cdot \mathbf{E} = 0, \qquad \mathbf{x} \in \partial\Omega_F, \quad \text{(far field BC's)}$$

$$(2.4) \qquad \mathbf{E}(\mathbf{x}, 0) = \mathbf{E}^{(0)}(\mathbf{x}), \quad \mathbf{E}_t(\mathbf{x}, 0) = \mathbf{E}_t^{(0)}(\mathbf{x}), \qquad \text{(initial conditions)}$$

where $\mathbf{E} = (E_x, E_y, E_z)$ and $c = 1/\sqrt{\epsilon\mu}$. The outward normal to the boundary $\partial\Omega$ is $\mathbf{n}$. At a boundary, $\partial\Omega_E$, next to a perfect electrical conductor (PEC), the boundary condition (BC) is that the tangential components of the field are zero, $\mathbf{n} \times \mathbf{E} = 0$. For boundaries where the computational domain is truncated, $\partial\Omega_F$, appropriate far-field boundary conditions are applied. These are denoted by $\mathcal{B}_F(\mathbf{E}) = 0$. The initial conditions should satisfy the constraints $\nabla \cdot \mathbf{E}^{(0)} = 0$ and $\nabla \cdot \mathbf{E}_t^{(0)} = 0$. Note that the second-order formulation requires the additional boundary condition $\nabla \cdot \mathbf{E} = 0$. The fact that Gauss's law, $\nabla \cdot \mathbf{E} = 0$, holds everywhere can be seen by noting that the divergence of the electric field, $\delta = \nabla \cdot \mathbf{E}$, satisfies a second order wave equation, $\delta_{tt} = c^2\Delta\delta$, with zero initial conditions and zero boundary conditions and thus δ will remain identically zero.

In two space dimensions the so-called TE$_Z$ mode (transverse electric mode with respect to z) is considered. Let $\mathbf{w} = (u, v, w) = (E_x, E_y, H_z)$ denote the vector holding the x- and y-components of the electric field and the z-component of the magnetic field. In addition, let $\mathbf{u} = (u, v) = (E_x, E_y)$. The initial boundary value problem for Maxwell's equations in this case is

$$(2.5) \qquad \partial_t^2 \mathbf{w} = c^2\Delta\mathbf{w} \qquad\qquad \mathbf{x} \in \Omega,$$

$$(2.6) \qquad \mathbf{u}(\mathbf{x}, 0) = \mathbf{u}^{(0)}(\mathbf{x}), \quad \mathbf{u}_t(\mathbf{x}, 0) = \mathbf{u}_t^{(0)}(\mathbf{x}), \quad t = 0, \qquad \text{(initial conditions)}$$

$$(2.7) \qquad w(\mathbf{x}, 0) = w^{(0)}(\mathbf{x}), \quad w_t(\mathbf{x}, 0) = w_t^{(0)}(\mathbf{x}), \quad t = 0, \qquad \text{(initial conditions)}$$

$$(2.8) \qquad \mathbf{n} \times \mathbf{u} = 0, \ \ \nabla \cdot \mathbf{u} = 0, \ \ \partial_n w = 0, \qquad \mathbf{x} \in \partial\Omega_E, \quad \text{(PEC BC's)}$$

$$(2.9) \qquad \mathcal{B}_F(\mathbf{w}) = 0, \ \ \nabla \cdot \mathbf{u} = 0, \qquad \mathbf{x} \in \partial\Omega_F. \quad \text{(far field BC's)}$$

As in three dimensions, the initial conditions should satisfy Gauss' law, $\nabla \cdot \mathbf{u}^{(0)} = 0$, $\nabla \cdot \mathbf{u}_t^{(0)} = 0$. In two dimensions it may be possible to solve for the one component $w = H_z$ or the two components, $\mathbf{u} = (E_x, E_y)$. However, all three components will be considered here in order to develop the numerical scheme for either case.

3. Summary of the numerical scheme. Consider the second-order wave equation with a forcing function, $u_{tt} = c^2\Delta u + f$. An attractive time stepping method to solve this second-order wave equation is the *modified equation* approach based on the Taylor series

$$u(\mathbf{x}, t+\Delta t) - 2u + u(\mathbf{x}, t-\Delta t) = 2\tfrac{\Delta t^2}{2!}\partial_t^2 u + 2\tfrac{\Delta t^4}{4!}\partial_t^4 u + 2\tfrac{\Delta t^6}{6!}\partial_t^6 u + \ldots\ .$$

Using the wave equation to eliminate even numbers of time derivatives in terms of space derivatives gives

(3.1) $u(\mathbf{x}, t + \Delta t) - 2u + u(\mathbf{x}, t - \Delta t) = 2\frac{\Delta t^2}{2!}\left(c^2 \Delta u + f\right)$

$$+ 2\frac{\Delta t^4}{4!}\left\{(c^2\Delta)^2 u + c^2\Delta f + f_{tt}\right\} + \dots .$$

This last expansion can be used to derive an approximation of any order that only uses three time levels. Letting $U_{\mathbf{i}}^n \approx u(\mathbf{x_i}, t^n)$ denote a discrete approximation to u at the grid point $\mathbf{x_i}$ and time $t^n = n\Delta t$, a fourth-order accurate approximation is

(3.2)
$$U_{\mathbf{i}}^{n+1} - 2U_{\mathbf{i}}^n + U_{\mathbf{i}}^{n-1} = \Delta t^2\left(c^2 \Delta_{4h} U_{\mathbf{i}}^n + f\right) + \frac{\Delta t^4}{12}\left(c^4 (\Delta^2)_{2h} U_{\mathbf{i}}^n + c^2 \Delta_{2h} f + f_{tt}\right),$$

where Δ_{mh} denotes some m^{th}-order approximation to the Laplace operator Δ and $(\Delta^2)_{mh}$ denotes a mth-order approximation to the square of the Laplace operator. The precise form of these approximations will be given in section 5. Using a second-order approximation for Δ^2 prevents the discrete stencil from becoming wider than that of the fourth-order approximation for Δ, while retaining the order of accuracy. Higher-order approximations follow easily. The modified equation time-stepping approach is related to the Numerov and Stoermer methods for ODEs [29] and for the second-order wave equation has been considered by numerous authors, including Dablain [6] and Bell and Shubin [39]. Anné et.al. [1] showed that in one space dimension the time step restriction required for stability is independent of the order of accuracy. Gustafsson and Mossberg [15] use a similar approach for treating the equations written as a first order system.

The time stepping scheme is not restricted to the modified equation approach. The spatial discretization and boundary conditions can be employed in a method-of-lines approach and used with any number of time stepping schemes for the second-order ODE $u_{tt} = F(u, t)$. High-order Stoermer approximations [29] have been implemented and used with success. Although these schemes require a smaller time step as the order of accuracy increases, the approach may be attractive such as to simplify the implementation details for the case of variable $\epsilon(\mathbf{x})$ and $\mu(\mathbf{x})$.

High-order accurate finite difference approximations that use wide stencils require special treatment at boundaries. One common approach for treating approximations near boundaries is to use one-sided difference approximations. Another approach, the one primarily taken here, is to use high-order accurate centered approximations to boundary conditions that use compatibility conditions derived from the continuous formulation [20, 14]. In particular, appropriate compatibility conditions for a PEC boundary are now given. The essential boundary conditions for a perfect electrical conductor are given by equation (2.2). By taking $2m$-time derivatives of these boundary conditions and using equations (2.1) it follows that

(3.3) $\mathbf{n} \times (\Delta^m \mathbf{E})(\mathbf{x}, t) = 0,$ $\nabla \cdot (\Delta^m \mathbf{E})(\mathbf{x}, t) = 0$ $\mathbf{x} \in \partial\Omega_E,$

for $m = 0, 1, 2, \dots$. In the two-dimensional case, taking $2m$-time derivatives of the Neumann boundary condition for H_z leads to the compatibility conditions

(3.4) $\partial_n \Delta^m H_z(\mathbf{x}, t) = 0,$ $\mathbf{x} \in \partial\Omega_E,$

for $m = 0, 1, 2, \dots$. Discrete approximations to the compatibility conditions (3.3–3.4) can be used as numerical boundary conditions. In general, the use of centered boundary conditions such as those based on these compatibility conditions, will be more stable and more accurate than boundary conditions based on one-sided differences.

In summary, the proposed scheme for Maxwell's equations uses the modified equation time-stepping approximation based on (3.1), such as equation (3.2) for a fourth-order scheme, together with discrete approximations to the boundary conditions (2.2) and compatibility conditions (3.3) or (3.4). These equations are discretized on an

overlapping grid. Symmetric difference approximations to the equations are developed in section 5. The solution values at the overlapping grid interpolation points are obtained using high-order accurate interpolation as described in section 4. On a Cartesian grid the basic scheme is neutrally stable and non-dissipative. From an analysis of similar problems [35], it can be expected that such a scheme may develop some weak instabilities near boundaries of curvilinear grids and near interpolation points of the overlapping grid. These instabilities are easily dealt with, however, by the addition of a high-order spatial dissipation. This dissipation does not change the accuracy of the scheme and can be added locally in regions near boundaries and interpolation points. Computational results show that this dissipation generally has a negligible effect on the overall accuracy of the solution, even for long times.

4. Overlapping grids. The governing equations for Maxwell's equations are discretized on an overlapping grid $\mathcal{G}$ (see Figures 7 and 10). The overlapping grid consists of a set of component grids, $\mathcal{G} = \{G_g\}$. The component grids overlap and cover the domain Ω. Typically, body fitted curvilinear grids are used near the boundaries while one or more background Cartesian grids are used in the remainder of the domain. Each component grid G_g is a logically rectangular, curvilinear grid in d space dimensions defined by a smooth mapping $\mathbf{x} = \mathbf{G}_g(\mathbf{r})$, from parameter space $\mathbf{r} \in [0,1]^d$ (the unit-square or unit-cube) to physical space $\mathbf{x} \in \mathbb{R}^d$. This mapping is used to define the location of grid points at any desired resolution. Derivatives of the mapping, $\partial \mathbf{x}/\partial \mathbf{r}$ will appear as coefficients in the discrete approximations, as shown in section 5. Thus, for high-order approximations it is important that the mapping $\mathbf{G}_g(\mathbf{r})$ be sufficiently smooth to avoid numerical artifacts such as spurious reflections. Points on a grid are classified as discretization points (where the PDE or boundary conditions are discretized), unused points and interpolation points (where the solution is interpolated from a different grid). The values of the solution at interpolation points are determined by a tensor-product Lagrange interpolant, using w points in each direction. For a pth-order approximation to the second-order wave equation, $p = 2, 4, ...$, the width of the interpolation stencil is taken as w $= p + 1$, following the analysis in [3]. Let $N_m^{(g)}$ grid denote the number of grid cells on grid G_g, in each coordinate direction, $m = 1, 2, ..., d$. Let $\mathbf{i} = (i_1, i_2, i_3)$ denote a multi-index, and let $\mathbf{x_i} = \mathbf{G}(\mathbf{r_i})$ denote the grid point corresponding to the unit square coordinate $\mathbf{r_i} = (i_1 \Delta r_1, i_2 \Delta r_2, i_3 \Delta r_3)$ where $i_m = 0, 1, ..., N_m$ and $\Delta r_m = 1/N_m$. Ghost points will correspond to $i_m = -1, -2, ...$ and $i_m = N_m + 1, N_m + 2, ...$ For more details on the discretization of problems on overlapping grids see [3, 21, 22].

Introduce a time step Δt, and let $U_{\mathbf{i}}^n$ denote a grid function at time $t^n = n\Delta t$, representing an approximation to $E_x(\mathbf{x_i}, t^n)$, for example. Introduce the standard forward, backward and centered divided difference operators in the r_1 direction by

$$D_{+r_1} U_{\mathbf{i}} = (U_{i_1+1,i_2,i_3} - U_{\mathbf{i}})/(\Delta r_1), \quad D_{-r_1} U_{\mathbf{i}} = (U_{\mathbf{i}} - U_{i_1-1,i_2,i_3})/(\Delta r_1),$$
$$D_{0r_1} U_{\mathbf{i}} = (U_{i_1+1,i_2,i_3} - U_{i_1-1,i_2,i_3})/(2\Delta r_1) \ .$$

Similar definitions hold for difference operators in the other coordinate directions, D_{+r_m}, D_{-r_m}, and D_{0r_m} for $m = 2, 3$. On a Cartesian grid, the grid spacings will be denoted by Δx, Δy and Δz with corresponding difference operators D_{+x}, D_{+y}, D_{+z} etc.. The difference operators in time are D_{+t}, D_{-t} and D_{0t} where for example $D_{+t} U_{\mathbf{i}}^n = (U_{\mathbf{i}}^{n+1} - U_{\mathbf{i}}^n)/\Delta t$.

5. High-order accurate symmetric difference approximations on curvilinear grids. In some applications, such as for long time integrations, it can be advantageous to use methods that are both high-order accurate and have low dissipation. To achieve these goals it will be helpful to use symmetric difference approximations to the discrete operators that are used in the solution of Maxwell's equations. Standard finite-difference approximations to the Laplace operator on curvilinear grids will not, in general, be symmetric. This section develops high-order accurate symmetric difference approximations for general logically-rectangular curvilinear grids.

To understand the relationship between symmetric approximations and low dis-

sipation schemes, consider the solution of the second-order wave equation,

$$(5.1) \qquad\qquad w_{tt} = \nabla \cdot (c^2 \nabla w),$$

for the function $w = w(\mathbf{x}, t)$ on a periodic domain $\Omega = [0, 2\pi]^d$. Let $(u, v) = \int_\Omega u^* v \, d\mathbf{x}$ and $\|u\| = (u, u)^{1/2}$ denote the usual L_2 inner product and norm on this domain. The wave equation (5.1) has no dissipation and there is an "energy" that remains constant over time. This energy can be determined by multiplying the equation by w_t, integrating over the domain and using integration by parts, giving

$$\tfrac{1}{2} \partial_t \left\{ \|w_t\|^2 + \|c\nabla w\|^2 \right\} = 0 \ .$$

The "energy" $\mathcal{E} = \|w_t\|^2 + \|c\nabla w\|^2$ is thus constant on a periodic domain. Discrete approximations to the wave equation (5.1) will not in general have a discrete energy that remains constant. For stability reasons many approximations will have some dissipation built into the spatial approximation or into the time stepping method. There are, however, a class of stable methods with no dissipation. Consider, for example, the second-order accurate centered approximation

$$(5.2) \qquad\qquad D_{+t}D_{-t}W_{\mathbf{i}}^n = c^2(D_{+,x}D_{-,x} + D_{+,y}D_{-,y})W_{\mathbf{i}}^n,$$

for use on a Cartesian grid, where $W_{\mathbf{i}}^n \approx w(\mathbf{x}_i, t^n)$. Let $(U, V)_h = \sum_{\mathbf{i}} U_{\mathbf{i}}^* V_{\mathbf{i}} \, \Delta x_1 \Delta x_2$ and $\|U\|_h = (U, U)_h^{1/2}$ denote the discrete L_2 inner product and norm on the Cartesian grid where the sum is over the grid points $i_m = 0, 1, ..., N_m - 1$. Equation (5.2) has a discrete "energy"

$$\mathcal{E}_h = \|D_{-t}W^n\|_h^2 + c^2(D_{-x}W^n, D_{-x}W^{n-1})_h + c^2(D_{-y}W^n, D_{-y}W^{n-1})_h,$$

that is conserved, as will be shown below. Equation (5.2) is a special case of the more general discrete approximation

$$(5.3) \qquad\qquad D_{+t}D_{-t}W^n = AW^n, \qquad n = 2, 3, 4, ...,$$

$$(5.4) \qquad\qquad W^0 = W^{(0)}, \quad W^1 = W^{(1)}, \quad \text{(initial conditions)},$$

where $W^n \in \mathbb{R}^N$ is the vector of all N grid point values $W_{\mathbf{i}}^n$, and $A \in \mathbb{R}^{N \times N}$ is the matrix representing the spatial discretization (including eliminated boundary conditions). The three-level time stepping schemes used in this paper are of this form (although for solutions on general overlapping grids a high-order dissipation is also added, section 9.2). The following lemma indicates the conditions on A so that all solutions to (5.3) remain uniformly bounded in time.

LEMMA 5.1. *The scheme (5.3- 5.4) is stable (the solutions remain uniformly bounded for all n) if and only if A has a complete set of eigenvectors, the eigenvalues λ of A are real and negative and Δt satisfies $-4 < \lambda \Delta t^2 < 0$ for all λ.*

Proof. Suppose that $\widehat{V}$ is an eigenvector of A corresponding to the eigenvalue λ. Looking for a solution of the form $V^n = \kappa^n \widehat{V}$ implies that κ satisfies the characteristic equation $\kappa - 2 + \kappa^{-1} = \lambda \Delta t^2$ with

$$(5.5) \qquad\qquad \kappa = 1 + \tfrac{1}{2}\lambda \Delta t^2 \pm \sqrt{(1 + \tfrac{1}{2}\lambda \Delta t^2)^2 - 1}.$$

When $\lambda = 0$ ($\kappa = 1$) or $\lambda \Delta t^2 = -4$ ($\kappa = -1$) there is a double root and the solutions can grow linearly in time, with $V^n = (c_0 + c_1(n\Delta t))\widehat{V}$, for $\lambda = 0$, and $V^n = (-1)^n (c_0 + c_1(n\Delta t))\widehat{V}$, for $\lambda \Delta t^2 = -4$. Therefore in these two cases the solutions will not be uniformly bounded for general initial conditions. A root, κ, of the characteristic equation will be a simple root and satisfy $|\kappa| = 1$ if and only if λ is real and $-4 < \lambda \Delta t^2 < 0$. In this case the solution will be of the form $V^n = (c_0 \kappa^n + c_1 \kappa^{-n})\widehat{V}$, and will remain uniformly bounded. If λ is not real or $\lambda > 0$ or $\lambda \Delta t^2 < -4$ there will be one root with $|\kappa| > 1$ and the approximation (5.3) is not uniformly bounded. If all λ satisfy $-4 < \lambda \Delta t^2 < 0$ and there is a complete set

of eigenvectors then the general solution can be represented as a linear combination of the eigenvectors and this solution will remain uniformly bounded. If there is not a complete set of eigenvectors then the Jordan normal form of A has a Jordan block of size larger than 1. In this case there are solutions of the form $V^n = (n\Delta t)\kappa^n$ and hence the solutions do not remain bounded in this case. $\square$

The conditions of lemma 5.1 will be satisfied when A is symmetric and the eigenvalues of A are less than zero. In this case a discrete energy estimate can be obtained as follows. Taking the inner product of $W^{n+1} - W^{n-1}$ with equation (5.3) and rearranging terms gives

$$\frac{1}{\Delta t^2}|W^{n+1} - W^n|^2 - \langle W^{n+1}, AW^n \rangle = \frac{1}{\Delta t^2}|W^n - W^{n-1}|^2 - \langle W^n, AW^{n-1} \rangle.$$

Here $\langle W, V \rangle = \sum_{i=1}^N W_i^* V_i$ and $|W| = \langle W, W \rangle^{\frac{1}{2}}$. It follows that the quantity

$$(5.6) \qquad \mathcal{E}_h^n = \frac{1}{\Delta t^2}|W^n - W^{n-1}|^2 - \langle W^n, AW^{n-1} \rangle$$

$$(5.7) \qquad = \frac{1}{\Delta t^2} \left\langle D_{+t}W^{n-1}, \left(I + \frac{\Delta t^2}{4}A\right)D_{+t}W^{n-1} \right\rangle - \langle W^{n-\frac{1}{2}}, AW^{n-\frac{1}{2}} \rangle$$

remains constant for all time, where $W^{n-\frac{1}{2}} := (W^n + W^{n-1})/2$. Note that two different time levels of the solution appear in the last term of equation (5.6). However, it can be seen from the alternative form (5.7) that $\mathcal{E}_h^n$ is positive provided Δt satisfies $-4 < \lambda\Delta t^2 < 0$ for all eigenvalues of A (see Kreiss et.al [28] or Cohen [4] for further details).

The above results provide a motivation for developing symmetric difference approximations for discretizations of Maxwell's equations. To this end, consider the generalized Laplace operator, L defined by

$$(5.8) \qquad\qquad Lw = \nabla \cdot (k\nabla w) .$$

A straight-forward approach to discretize L on a curvilinear grid is to use the mapping method, as follows. Using the chain rule, the operator L can be written in general curvilinear coordinates (with summation convention) as

$$(5.9) \qquad Lw = k(\mathbf{r})\frac{\partial r_n}{\partial x_i}\frac{\partial r_m}{\partial x_i}\frac{\partial^2 w}{\partial r_m \partial r_n} + \frac{\partial r_n}{\partial x_i}\left\{k(\mathbf{r})\frac{\partial}{\partial r_n}\left(\frac{\partial r_m}{\partial x_i}\right) + \frac{\partial k}{\partial r_n}\frac{\partial r_m}{\partial x_i}\right\}\frac{\partial w}{\partial r_m}.$$

The metric terms $\partial r_m/\partial x_n$ are computed from the mapping that defines the grid and are thus assumed to be known. The derivatives with respect to the parameter space coordinates r_m can be approximated with central difference approximations. Standard finite difference approximations, FDm, of order m, for $m = 2, 4, 6, ...$, can be defined in this way. The resulting approximations will not, however, be symmetric on general curvilinear grids. High-order accurate symmetric approximations on rectangular grids and unstructured grids have been developed for this type of operator by various authors, see for example [4, 16]. In the remainder of this section, it will be shown how to construct high-order accurate symmetric approximations to L for arbitrary curvilinear grids.

The operator L can be written in *conservation* form, or *self-adjoint* form, in general curvilinear coordinates as

$$(5.10) \qquad Lw = \frac{1}{J}\sum_{m=1}^d\sum_{n=1}^d \frac{\partial}{\partial r_m}\left(A^{mn}\frac{\partial w}{\partial r_n}\right), \qquad A^{mn} = kJ\sum_{\mu=1}^d\sum_{\nu=1}^d \frac{\partial r_m}{\partial x_\mu}\frac{\partial r_n}{\partial x_\nu},$$

where J denotes the determinant of the Jacobian matrix $[\partial x_i/\partial r_j]$. To improve readability in the subsequent discussion let $(r, s) = (r_1, r_2)$ and $(h_r, h_s) = (\Delta r_1, \Delta r_2)$. The discrete inner product on a curvilinear grid is defined as

$$(5.11) \qquad\qquad (U_\mathbf{i}, V_\mathbf{i})_h = \sum_\mathbf{i} U_\mathbf{i}^* V_\mathbf{i} \, J_\mathbf{i} \, h_r h_s .$$

Consider approximations to the two operators, $\mathcal{L}_{rr} = J^{-1}\partial_r(a\partial_r)$ and $\mathcal{L}_{rs} = J^{-1}\partial_r(b\partial_s)$ that are representative of the terms appearing in the expression (5.10) for L. The

operator $\mathcal{L}_{rr}$ will be approximated in the discrete form $\mathcal{L}_{rr}w = J^{-1}\partial_r(a\partial_r w) \approx J^{-1}\mathcal{D}_+(a_{i-\frac{1}{2}}\mathcal{D}_-)w(\mathbf{r_i})$, where $\mathcal{D}_+ \approx \partial_r w(r + h_r/2)$ and $\mathcal{D}_- \approx \partial_r w(r - h_r/2)$ are some appropriately defined high-order accurate approximations to the derivatives at locations midway between grid points and $a_{i-\frac{1}{2}} \approx a(r - h_r/2)$. If the adjoint of $J^{-1}\mathcal{D}_+$, with respect to (5.11), is $-J^{-1}\mathcal{D}_-$, then a a symmetric approximation will result since

$$(v, J^{-1}\mathcal{D}_+(a_{i-\frac{1}{2}}\mathcal{D}_-)w)_h = -(J^{-1}\mathcal{D}_-, a_{i-\frac{1}{2}}\mathcal{D}_-w)_h = (J^{-1}\mathcal{D}_+(a_{i-\frac{1}{2}}\mathcal{D}_-)v, w)_h.$$

To simplify notation let $D_+ = D_{+,r}$ and $D_- = D_{-,r}$. An order $2m+2$ approximation for $\mathcal{D}_+$ is obtained from the expansion

$$\tfrac{\partial w}{\partial r}(r + h_r/2) = D_+\left[1 + \sum_{n=1}^m \alpha_n h_r^{2n}(D_+D_-)^n\right]w(r + h_r/2) + \mathcal{O}(h_r^{2m+2}),$$

where the coefficients α_i can be determined from equating coefficients in the expression $y = \sin(y)\left[1 + \sum_{n=1}^\infty \alpha_n(-4\sin^2(y))^n\right]$, (see for example [12] or [14]). The first four values of α_i are given by $\alpha_1 = -\tfrac{1}{6}$, $\alpha_2 = \tfrac{3}{640}$, $\alpha_3 = -\tfrac{5}{7168}$, and $\alpha_4 = \tfrac{35}{294912}$. Assuming that the coefficient $a(r)$ is given at the grid points, a_i, approximations to $a_{i-1/2}$ will be needed. These approximations can be obtained by interpolation in a straight-forward fashion and to order $m = 2$, and 4 are given by

$$a_{i-1/2}^{(2)} = \tfrac{1}{2}(a_i + a_{i-1}), \quad a_{i-1/2}^{(4)} = \tfrac{9}{16}(a_i + a_{i-1}) - \tfrac{1}{16}(a_{i+1} + a_{i-2}),$$

where $a_{i-1/2}^{(m)} = a_{i-1/2} + O(h_r^m)$. Note that other forms of interpolation may be appropriate when the coefficient k is discontinuous. Define $\mathcal{D}_+$ and $\mathcal{D}_-$ as

$$\mathcal{D}_\pm = D_\pm\left[1 + \sum_{n=1}^\infty \alpha_n h_r^{2n}(D_+D_-)^n\right] .$$

Expanding the expression $\mathcal{D}_+(a\mathcal{D}_-)$ in powers of h_r^2 leads to

$$\tfrac{\partial}{\partial r}\left(a\tfrac{\partial}{\partial r}\right) = D_+(a_{i-1/2}^{(m)}D_-) - \tfrac{h_r^2}{24}\left[D_+(a_{i-1/2}^{(m-2)}D_+D_-^2) + D_+^2D_-(a_{i-1/2}^{(m-2)}D_-)\right]$$
$$+ \tfrac{h_r^4}{24^2}\left[D_+^2D_-(a_{i-1/2}^{(m-4)}D_+D_-^2)\right] + \tfrac{3h_r^4}{640}\left[D_+(a_{i-1/2}^{(m-4)}D_+^2D_-^3) + D_+^3D_-^2(a_{i-1/2}^{(m-4)}D_-)\right]$$

(5.12)

$$- \tfrac{5h_r^6}{7168}\left[D_+^4D_-^3(a_{i-1/2}^{(m-6)}D_-) + D_+(a_{i-1/2}^{(m-6)}D_+^3D_-^4)\right]$$
$$- \tfrac{3h_r^6}{640\cdot24}\left[D_+^2D_-(a_{i-1/2}^{(m-6)}D_+^2D_-^3) + D_+^3D_-^2(a_{i-1/2}^{(m-6)}D_+D_-^2)\right] + O(h_r^8)$$

Note that different orders of approximation for $a_{i-1/2}$ are used, so that the difference stencil for a mth-order formulation is no larger than $m+1$ points wide in each direction. Equation (5.12) can be used to generate symmetric approximations of order m by involving terms up to and including those of order h_r^m. For example, a fourth-order symmetric approximation to $J^{-1}\partial_r(a\partial_r)$ is

$$\mathcal{L}_{rr}^{(4)}[a]w := J_{\mathbf{i}}^{-1}\left\{D_+(a_{i-1/2}^{(4)}D_-) - \tfrac{h_r^2}{24}\left[D_+(a_{i-1/2}^{(2)}D_+D_-^2) + D_+^2D_-(a_{i-1/2}^{(2)}D_-)\right]\right\}w.$$

It is easy to show that the approximation $\mathcal{L}_{rr}^{(4)}[a]$ is symmetric since the adjoint of $J^{-1}D_+$ is $-J^{-1}D_-$, with respect to the discrete inner product (5.11)).

The operator $\mathcal{L}_{rs} = J^{-1}\partial_r(b\partial_s)$ for the mixed derivative terms, is approximated using

$$(5.13)\quad \mathcal{L}_{rs} \approx J^{-1}D_{0r}\left[1 + \sum_{n=1}^\infty \beta_n h_r^{2n}(D_{+r}D_{-r})^n\right]\left\{bD_{0s}\left[1 + \sum_{n=1}^\infty \beta_n h_s^{2n}(D_{+s}D_{-s})^n\right]\right\},$$

where $D_{+r} = D_{+,r_1}$, $D_{+s} = D_{+,r_2}$ etc.. and where $b = b_{\mathbf{i}}$ denotes the value of b at a grid point. In this case the values of b that appear are located at the grid points and no interpolation is needed. From the expansion of (5.13), a fourth-order approximation to $J^{-1}\partial_r(b\partial_s)$ is

$$\mathcal{L}_{rs}^{(4)}[b]w := J_{\mathbf{i}}^{-1}\left\{D_{0r}(bD_{0s}) - \tfrac{1}{6}\left[h_s^2D_{0r}(bD_{+s}D_{-s}D_{0s}) + h_r^2D_{0r}D_{+r}D_{-r}(bD_{0s})\right]\right\}w.$$
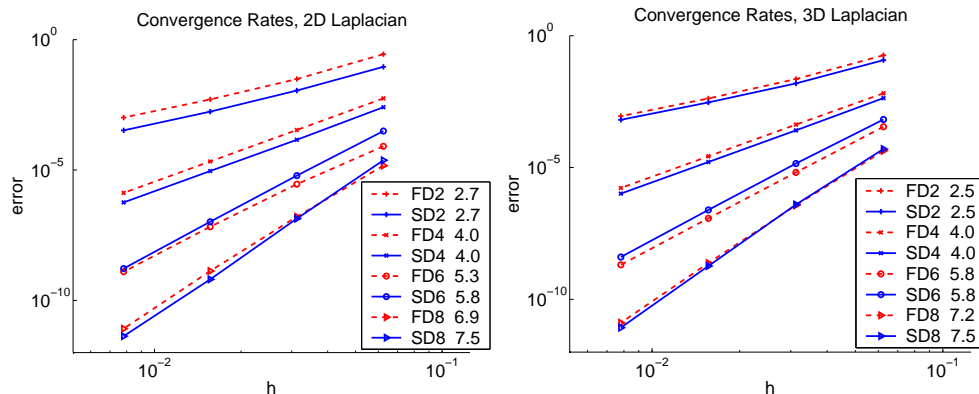
FIG. 1. *Convergence rates for the maximum-norm errors in computing the Laplacian on a smooth non-orthogonal grid. FDm denotes the standard finite difference approximations of order m while SDm denotes the symmetric difference approximations of order m. The estimated convergence rate for each approximation is indicated in the legend.*

This operator is not symmetric, but the combination $\mathcal{L}_{rs}^{(4)}[b] + \mathcal{L}_{sr}^{(4)}[b]$ will be symmetric. A fourth-order symmetric approximation to $L = \nabla \cdot (k\nabla)$ denoted by $\mathcal{L}^{(4)}$ is thus

$$\mathcal{L}^{(4)} = \sum_{m=1}^{d} \sum_{n=1}^{d} \mathcal{L}_{r_m r_n}^{(4)}[A^{mn}] \ .$$

where the coefficients A^{mn} are defined by (5.10) The symmetric approximation can be easily generalized to the case where $k(\mathbf{x})$ is replaced by a symmetric tensor; this only changes the definition of A^{mn}.

The symmetric approximations have been implemented in two and three space dimensions for orders $m = 2$, 4, 6, and 8. Figure 1 compares the accuracy of the symmetric difference operators of order m, denoted by SDm to those of the standard finite difference operators of order m, denoted by FDm. The maximum-norm errors in computing the Laplacian of a trigonometric function on a smooth non-orthogonal grid are presented in the figure for a sequence of grids of increasing resolution. The estimated convergence rate for each approximation is also indicated. These estimated rates are computed from a least squares fit to the log of the error versus the log of the grid spacing. The results show that the symmetric schemes, SDm, have similar errors to the finite difference schemes, FDm. The convergence rates are reasonably close to the expected values. Note that the numerical values of the computed rates are sensitive to small changes in the data.

To illustrate that the discrete operators SDm are indeed symmetric on arbitrary logically-rectangular grids, a computation was performed on the grid shown in Figure 2. The grid for the unit square, with periodic boundary conditions, is obtained by randomly perturbing the grid points of a Cartesian grid. The grid points are defined as $\mathbf{x_i} = ((i_1 + \mathcal{R}^{(x)}/4)\Delta x, (i_2 + \mathcal{R}^{(y)}/4)\Delta y)$ where $\mathcal{R}^{(x)}$ and $\mathcal{R}^{(y)}$ are pseudo-random numbers uniformly distributed in $[-1, 1]$. Figure 2 shows the results from computations solving Maxwell's equations with $c = 1$ on a two-dimensional perturbed square. The discrete energy (5.6) for the component E_x (other components are similar) is plotted for different schemes for $t \in [0, 100]$. Let the symmetric time-stepping schemes be denoted by TnSDm where n is the order of accuracy in time and m is the order of accuracy in space. Figure 2 presents results for the methods T2SD2, T4SD4, T2SD6 and T2SD8. The scheme T4SD4 is given by equation (3.2). The schemes T2SDm use second-order accurate time stepping with an mth order accurate approximation to the Laplacian, $U_{\mathbf{i}}^{n+1} - 2U_{\mathbf{i}}^{n} + U_{\mathbf{i}}^{n-1} = \Delta t^2 c^2 \Delta_{mh} U_{\mathbf{i}}^{n}$. The discrete energy is essentially constant over the computation (to within a relative error of about 10^{-10} in 64 bit double precision) for all schemes that use the symmetric operators. By comparison, schemes using the standard finite difference approximations, denoted by TmFDn are not energy preserving. These schemes are not stable for this grid without the addition of some dissipation. Figure 2 also shows the corresponding results for a perturbed three-dimensional box.
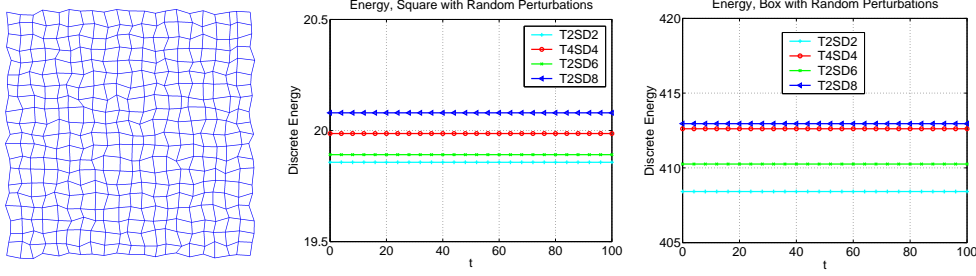
FIG. 2. *The computation of Maxwell's equations on a randomly perturbed Cartesian grid using the symmetric approximations. The discrete energy remains almost constant (to a relative error of about 10^{-10} in double precision) using the symmetric difference approximations, even on a non-smooth, non-orthogonal grid. Results for a perturbed grid for a square and a perturbed grid for a box are shown for the various schemes TmSDn of order of accuracy n in time and m in space.*

6. Analysis of the scheme. In this section the stability of the fourth-order accurate time stepping scheme and boundary conditions is analyzed for a model problem. The analysis considers the solution to Maxwell's equations on the unit square, $\Omega = [0,1]^2$, with PEC boundary conditions at $x = 0$ and $x = 1$ and periodic boundary conditions in y. A Cartesian grid is introduced with mesh points $\mathbf{x_i} = (x_i, y_j) = (i\Delta x, j\Delta y)$, where $\mathbf{i} = (i,j)$ and $i = -2, 1, 0, 1, 2, ..., N_1, N_1 + 1, N_1 + 2$ with $\Delta x = 1/N_1$, and $j = 0, 1, 2, ..., N_2 - 1$, with $\Delta y = 1/N_2$. Two lines of ghost points have been introduced outside the boundaries at $x = 0$ and $x = 1$. Discrete approximations to $E_x(\mathbf{x_i}, t^n)$ and $E_y(\mathbf{x_i}, t^n)$ are given by U_{ij}^n and V_{ij}^n, respectively, with $\mathbf{U_i^n} = (U_\mathbf{i}^n, V_\mathbf{i}^n)$. For this two-dimensional example the discretization for the magnetic field will not be presented since it is the same as the discretization for E_x. The interior equations (2.5) are discretized in a fourth-order manner using the modified equation approximation (3.2)

$$(6.1) \quad \mathbf{U_i}^{n+1} - 2\mathbf{U_i}^n + \mathbf{U_i}^{n-1} = (c\Delta t)^2 \Delta_{4h} \mathbf{U_i}^n + \frac{(c\Delta t)^4}{12} \Delta_{2h}^2 \mathbf{U_i}^n,$$
$$\text{for} \quad i = 0, 1, ..., N_1, j = 0, 1, .., N_2 - 1.$$

Here Δ_{4h} is a fourth-order approximation to Δ and Δ_{2h}^2 is a second-order approximation to Δ^2 given by

$$\Delta_{4h} \equiv D_{+x}D_{-x}\left(1 - \frac{\Delta x^2}{12}D_{+x}D_{-x}\right) + D_{+y}D_{-y}\left(1 - \frac{\Delta y^2}{12}D_{+y}D_{-y}\right),$$
$$\Delta_{2h}^2 \equiv \left(D_{+x}D_{-x} + D_{+y}D_{-y}\right)^2.$$

The divided difference operators D_{+x}, D_{-x}, D_{0x} etc. were defined in section 4. The boundary conditions at $x = 0$ ($i = 0$) and $x = 1$ ($i = N_1$) are discretized as

$$(6.2) \qquad\qquad\qquad V_\mathbf{i}^n = 0, \qquad \text{for } i = 0, N_1,$$

$$(6.3) \qquad D_{0x}\left(1 - \frac{\Delta x^2}{6}D_{+x}D_{-x}\right)U_\mathbf{i}^n = 0, \qquad \text{for } i = 0, N_1,$$

$$(6.4) \qquad D_{+x}D_{-x}\left(1 - \frac{\Delta x^2}{12}D_{+x}D_{-x}\right)V_\mathbf{i}^n = 0, \qquad \text{for } i = 0, N_1,$$

$$(6.5) \qquad\qquad D_{0x}D_{+x}D_{-x}U_\mathbf{i}^n = 0, \qquad \text{for } i = 0, N_1,$$

$$(6.6) \qquad\qquad \left(D_{+x}D_{-x}\right)^2 V_\mathbf{i}^n = 0, \qquad \text{for } i = 0, N_1,$$

where three additional *numerical boundary conditions* have been introduced. The boundary conditions (6.2-6.6) are, respectively, approximations to $E_y = 0$, fourth-order approximations to $\nabla \cdot \mathbf{E} = 0$, $\Delta E_y = 0$, and second-order approximations to $\nabla \cdot \Delta \mathbf{E} = 0$ and $\Delta^2 E_y = 0$. The latter three equations arise from the compatibility conditions (3.3). The scheme is completed by specifying initial values for two time levels, for example,

$$(6.7) \qquad \mathbf{U}_{ij}^0 = \mathbf{E}^{(0)}(\mathbf{x}_{ij}),$$

$$(6.8) \qquad \mathbf{U}_{ij}^1 = \mathbf{E}^{(0)}(\mathbf{x}_{ij}) + \Delta t \mathbf{E}_t^{(0)}(\mathbf{x}_{ij}) + \frac{\Delta t^2}{2}\Delta_{2h}\mathbf{E}^{(0)}(\mathbf{x}_{ij}) + \frac{\Delta t^3}{3!}\Delta_{2h}\mathbf{E}_t^{(0)}(\mathbf{x}_{ij}).$$

LEMMA 6.1. *The solution to the discrete approximation to the vector wave equation* (6.1) *with boundary conditions* (6.2-6.6) *is stable (the solutions remain uniformly bounded) provided*

$$(6.9) \qquad \Delta t < c^{-1} \left(\Delta x^{-2} + \Delta y^{-2} \right)^{-1/2}.$$

Proof. Making the ansatz $\widetilde{U}_{\mathbf{i}}^n = \kappa^n \cos(\alpha \pi x_i) e^{i2\pi\beta y_j}$ and $\widetilde{V}_{\mathbf{i}}^n = \kappa^n \sin(\alpha \pi x_i) e^{i2\pi\beta y_j}$ it follows that $\widetilde{U}_{\mathbf{i}}^n$, and $\widetilde{V}_{\mathbf{i}}^n$ satisfy equations (6.1) and boundary conditions (6.2-6.6) provided κ satisfies the characteristic equation

$$(6.10) \qquad \kappa - 2 + \kappa^{-1} = -4G$$

where $\xi_x = \pi\alpha\Delta x$, $\xi_y = 2\pi\beta\Delta y$, $\sigma_x = \sin^2(\xi_x/2)$, $\sigma_y = \sin^2(\xi_y/2)$, $\lambda_x = c\frac{\Delta t}{\Delta x}$, $\lambda_y = c\frac{\Delta t}{\Delta y}$ and

$$G = \lambda_x^2\sigma_x[1 + \tfrac{1}{3}\sigma_x] + \lambda_y^2\sigma_y[1 + \tfrac{1}{3}\sigma_y] - \tfrac{1}{3}[\lambda_x^2\sigma_x + \lambda_y^2\sigma_y]^2,$$
$$\alpha = 0, 1, 2, ..., N_1, \quad \beta = 0, 1, 2, ..., N_2 - 1.$$

The two roots of the characteristic equation (6.10) are $\kappa_\pm = (1-2G)\pm\sqrt{(1 - 2G)^2 - 1}$ where $\kappa_+ = \kappa_-^{-1}$. The roots will satisfy $|\kappa_\pm| = 1$ and the solutions will remain uniformly bounded provided $0 < G < 1$ (following the argument in the proof of lemma 5.1). Letting $\gamma = \lambda_x^2\sigma_x + \lambda_y^2\sigma_y$ it follows that G can be written in the form

$$G = \gamma - \tfrac{1}{3}\gamma^2 + \tfrac{1}{3}(\lambda_x^2\sigma_x^2 + \lambda_y^2\sigma_y^2),$$
$$\le \gamma - \tfrac{1}{3}\gamma^2 + \tfrac{1}{3}(\lambda_x^2\sigma_x + \lambda_y^2\sigma_y) = \gamma + \tfrac{1}{3}\gamma(1 - \gamma).$$

The function G is always positive for $0 < \gamma < 1$. The function $\widetilde{G}(\gamma) = \gamma + \tfrac{1}{3}\gamma(1-\gamma)$ is less than 1 for $0 < \gamma < 1$ and thus $0 < G < 1$ provided $\gamma < 1$. Therefore the condition that $\widetilde{U}_{\mathbf{i}}^n$ and $\widetilde{V}_{\mathbf{i}}^n$ remain uniformly bounded is

$$(6.11) \qquad \lambda_x^2\sigma_x + \lambda_y^2\sigma_y \le \lambda_x^2 + \lambda_y^2 < 1,$$

Let $\kappa_{\alpha,\beta}$ and $G_{\alpha,\beta}$ denote the values of κ_+ and G as functions of α and β. The general solution can be written as

$$U_{\mathbf{i}}^n = \sum_\alpha \sum_\beta (A_{\alpha,\beta}\kappa_{\alpha,\beta}^n + B_{\alpha,\beta}\kappa_{\alpha,\beta}^{-n}) \cos(\alpha\pi x_{\mathbf{i}}) e^{i2\beta\pi y_{\mathbf{i}}},$$
$$V_{\mathbf{i}}^n = \sum_\alpha \sum_\beta (C_{\alpha,\beta}\kappa_{\alpha,\beta}^n + D_{\alpha,\beta}\kappa_{\alpha,\beta}^{-n}) \sin(\alpha\pi x_{\mathbf{i}}) e^{i2\beta\pi y_{\mathbf{i}}},$$

where the values of $A_{\alpha,\beta}$, $B_{\alpha,\beta}$, $C_{\alpha,\beta}$ and $D_{\alpha,\beta}$ are determined by the initial conditions. The solution will be stable provided $0 < G_{\alpha,\beta} < 1$ for all permissible α, β. It follows from the stability condition (6.11) and the definitions of λ_x and λ_y that the solution to the model problem is stable provided the time step satisfies (6.9). $\square$.

Note that

$$\kappa_{\alpha,\beta} = 1 + ik\Delta t + \tfrac{1}{2}(ik\Delta t)^2 + \tfrac{1}{3!}(ik\Delta t)^3 + \tfrac{1}{4!}(ik\Delta t)^4 + O(\Delta t h^4, \Delta t^3 h^2, \Delta t^5)$$

where $h = \sqrt{\Delta x^2 + \Delta y^2}$, $k = \sqrt{k_x^2 + k_y^2}$, $k_x = \pi\alpha$, and $k_y = 2\pi\beta$. This shows that κ_{mn} is a fourth-order accurate approximation to $e^{ik\Delta t}$. The discrete eigenfunctions $\widetilde{U}_{\mathbf{i}}^n$ and $\widetilde{V}_{\mathbf{i}}^n$ are thus fourth-order accurate approximations to the eigenfunctions of the continuous problem, and it is apparent that the discrete approximation to the model problem is fourth-order accurate.

In three dimensions an argument similar to that used for the two-dimensional case shows that the stability condition is $\Delta t < c^{-1} \left(\Delta x^{-2} + \Delta y^{-2} + \Delta z^{-2} \right)^{-1/2}$.

6.1. Relationship to the Yee Scheme. The current approach can be compared to the classic Yee scheme [44]. For the 2D TE_Z system

$$u_t = w_y, \quad v_t = -w_x, \quad w_t = u_y - v_x,$$

the Yee scheme can be written as

(6.12) $$D_{+t}U^n_{i+\frac{1}{2},j} = D_{+y}W^{n+\frac{1}{2}}_{i+\frac{1}{2},j-\frac{1}{2}},$$

(6.13) $$D_{+t}V^n_{i,j+\frac{1}{2}} = -D_{+x}W^{n+\frac{1}{2}}_{i-\frac{1}{2},j+\frac{1}{2}},$$

(6.14) $$D_{+t}W^{n-\frac{1}{2}}_{i+\frac{1}{2},j+\frac{1}{2}} = D_{-y}U^n_{i+\frac{1}{2},j} - D_{-x}V^n_{i,j+\frac{1}{2}},$$

where the subscripts denote the staggering of the variables with $W^{n+\frac{1}{2}}_{i+\frac{1}{2},j+\frac{1}{2}}$, for example, being cell-centered. It is also true that $D_{+x}U^n_{i+\frac{1}{2},j} + D_{+y}V^n_{i,j+\frac{1}{2}} = 0$ (assuming the initial conditions satisfy this). A discrete second-order form for these equations can be found by first applying the operator D_{-t} to equation (6.12). Combining this with the other equations gives

$$D_{+t}D_{-t}U^n_{i+\frac{1}{2},j} = D_{+y}D_{-y}U^n_{i+\frac{1}{2},j} - D_{+y}D_{+x}V^n_{i-\frac{1}{2},j+\frac{1}{2}},$$
$$= (D_{+x}D_{+x} + D_{+y}D_{-y})U^n_{i+\frac{1}{2},j},$$

and similarly for the other variables. Thus each component satisfies the second-order wave equation discretized with the standard central difference operators. Neglecting boundaries, the Yee scheme therefore effectively uses the same discretization as the second-order accurate version of the current scheme.

7. Boundary conditions at material interfaces. In this section the propagation of electromagnetic waves through different dielectric (insulating) materials will be considered. The domain Ω is partitioned into a set of sub-domains, $\Omega = \bigcup_k \Omega_k$, with each Ω_k representing a region with different material properties,

$$\epsilon(\mathbf{x}) = \epsilon_k, \quad \mu(\mathbf{x}) = \mu_k, \quad \text{for } \mathbf{x} \in \Omega_k.$$

The assumption is made that ϵ and μ are constant within each sub-domain (although this restriction is not essential). The boundaries of each sub-domain, $\partial\Omega_k$, are assumed to be sufficiently smooth so that normal and tangent vectors to the interface can be defined. Overlapping grids will be used to discretize each sub-domain separately. The sub-domain boundaries will be represented with boundary fitted grids (see for example Figure 7). Maxwell's equations in second-order form are discretized in each sub-domain using the high-order accurate difference approximations discussed in previous sections. Ghost points are used on the grids on both sides of the interface as shown in the one-dimensional overlapping grid of Figure 3. Boundary conditions at the interface are required for the numerical approximation. These boundary conditions are used to determine the solution values at the ghost points. As in the case of the PEC boundary, centered numerical boundary conditions are developed from compatibility conditions consistent with the governing equations. The compatibility conditions are based on interface jump conditions derived from the first order form of Maxwell's equations. For $\rho = 0$, with variable ϵ and μ, these are

(7.1) $$\epsilon(\mathbf{x})\mathbf{E}_t = \nabla \times \mathbf{H}, \qquad \mu(\mathbf{x})\mathbf{H}_t = -\nabla \times \mathbf{E},$$

(7.2) $$\nabla \cdot (\epsilon(\mathbf{x})\mathbf{E}) = 0, \qquad \nabla \cdot (\mu(\mathbf{x})\mathbf{H}) = 0.$$

Under the assumption that $\mathbf{E}$ and $\mathbf{H}$ remain bounded, the basic jump conditions at a material interface $\mathcal{I}$ are derived by integrating each of the equations (7.1-7.2) over an appropriate control volume that spans the interface, (see for example [2]), and the result is

(7.3) $$[\epsilon\mathbf{n} \cdot \mathbf{E}]_{\mathcal{I}} = 0, \qquad [\mu\mathbf{n} \cdot \mathbf{H}]_{\mathcal{I}} = 0,$$

(7.4) $$[\boldsymbol{\tau}_m \cdot \mathbf{E}]_{\mathcal{I}} = 0, \qquad [\boldsymbol{\tau}_m \cdot \mathbf{H}]_{\mathcal{I}} = 0.$$

Here $[\mathbf{f}]_{\mathcal{I}}$ denotes the jump in $\mathbf{f}$ across the interface, $\mathbf{n} = \mathbf{n}(\mathbf{x})$ is the unit normal vector to the interface and $\boldsymbol{\tau}_m = \boldsymbol{\tau}_m(\mathbf{x})$ is a unit tangent vector to the material interface. Since there are two linearly independent tangents in three dimensions, there will be two linearly independent conditions $[\boldsymbol{\tau}_m \cdot \mathbf{E}] = 0$, $m = 1, 2$ (or just one condition in two dimensions). Jump conditions on the first spatial derivatives of the solution follow directly from equations (7.2), and also by taking one time derivative of (7.4) and combining with equations (7.1),

$$(7.5) \qquad\qquad [\nabla \cdot \mathbf{E}]_{\mathcal{I}} = 0, \qquad [\nabla \cdot \mathbf{H}]_{\mathcal{I}} = 0,$$

$$(7.6) \qquad\qquad [\mu^{-1}\boldsymbol{\tau}_m \cdot \nabla \times \mathbf{E}]_{\mathcal{I}} = 0, \qquad [\epsilon^{-1}\boldsymbol{\tau}_m \cdot \nabla \times \mathbf{H}]_{\mathcal{I}} = 0.$$

Note that $[\nabla \cdot (\epsilon \mathbf{E})]_{\mathcal{I}} = 0$ can be replaced by $[\nabla \cdot \mathbf{E}]_{\mathcal{I}} = 0$ since $\nabla \cdot \mathbf{E}$ is identically zero on either side of the interface. A similar remark applies to the condition $[\nabla \cdot \mathbf{H}]_{\mathcal{I}} = 0$. Additional compatibility conditions can be derived by taking an even number of time derivatives of the four conditions (7.3-7.6) and using the vector wave equation (1.6) to transform the time derivatives into space derivatives. This gives the complete set of interface conditions

$$(7.7) \qquad\qquad [\epsilon\mathbf{n} \cdot \Delta^n \mathbf{E}/(\epsilon\mu)^n]_{\mathcal{I}} = 0, \qquad [\mu\mathbf{n} \cdot \Delta^n \mathbf{H}/(\epsilon\mu)^n]_{\mathcal{I}} = 0,$$

$$(7.8) \qquad\qquad [\boldsymbol{\tau} \cdot \Delta^n \mathbf{E}/(\mu\epsilon)^n]_{\mathcal{I}} = 0, \qquad [\boldsymbol{\tau} \cdot \Delta^n \mathbf{H}/(\mu\epsilon)^n]_{\mathcal{I}} = 0,$$

$$(7.9) \qquad\qquad [\nabla \cdot (\Delta^n \mathbf{E})]_{\mathcal{I}} = 0, \qquad [\nabla \cdot (\Delta^n \mathbf{H})]_{\mathcal{I}} = 0,$$

$$(7.10) \qquad [\mu^{-1}\boldsymbol{\tau} \cdot \nabla \times \Delta^n \mathbf{E}/(\mu\epsilon)^n]_{\mathcal{I}} = 0, \qquad [\epsilon^{-1}\boldsymbol{\tau} \cdot \nabla \times \Delta^n \mathbf{H}/(\mu\epsilon)^n]_{\mathcal{I}} = 0,$$

for $n = 0, 1, 2, 3, \ldots$. These interface jump conditions impose constraints on each spatial derivative of the solution.

Discrete versions of the jump conditions are used as numerical boundary conditions in the following manner. First consider the case of a second-order accurate approximation that uses one ghost line on each side of the interface. Let $\mathbf{U}_{\mathbf{i}}^{(k)}$ denote the discrete approximation to the electric field where $k = 1, 2$, denotes the solution on each side of the material interface. The dependence of the solution on time is suppressed for this discussion. To be specific, let the interface correspond to the value of $i_1 = 0$ and the ghost line values correspond to $i_1 = -1$. The values $\mathbf{U}_{-1,i_2,i_3}^{(1)}$ and $\mathbf{U}_{-1,i_2,i_3}^{(2)}$ of the solution on the ghost lines, (one ghost line value on each side of the interface) are determined by imposing the following centered interface conditions at $i_1 = 0$,

$$(7.11) \qquad [\epsilon\mathbf{n} \cdot \Delta_{2h}\mathbf{U}_{\mathbf{i}}^{(k)}/(\epsilon\mu)]_{\mathcal{I}} = 0, \qquad [\boldsymbol{\tau}_m \cdot \Delta_{2h}\mathbf{U}_{\mathbf{i}}^{(k)}/(\mu\epsilon)]_{\mathcal{I}} = 0,$$

$$(7.12) \qquad [\nabla_{2h} \cdot (\mathbf{U}_{\mathbf{i}}^{(k)})]_{\mathcal{I}} = 0, \qquad [\mu^{-1}\boldsymbol{\tau}_m \cdot \nabla_{2h} \times \mathbf{U}_{\mathbf{i}}^{(k)}]_{\mathcal{I}} = 0.$$

Here $\nabla_{2h}\cdot$, $\nabla\times_{2h}$, and Δ_{2h} are some appropriate second-order accurate centered difference approximations. Equations (7.11-7.12) implicitly specify that the time derivatives of the jump conditions (7.3-7.4) are zero (to second-order accuracy). Therefore, by imposing the conditions (7.11-7.12) the basic jump conditions (7.3-7.4) should also be approximately satisfied (assuming they are satisfied at the initial time). Therefore it may not be essential to explicitly impose the conditions (7.3-7.4). In practice, however, the solution values on the interface itself are constrained to satisfy the basic jump conditions,

$$(7.13) \qquad\qquad [\epsilon\mathbf{n} \cdot \mathbf{U}_{\mathbf{i}}^{(k)}]_{\mathcal{I}} = 0, \qquad [\boldsymbol{\tau}_m \cdot \mathbf{U}_{\mathbf{i}}^{(k)}]_{\mathcal{I}} = 0.$$

by setting the solution values on the side of the interface with the larger value of ϵ in terms of the values on the other side. For example, if $\epsilon_2 \leq \epsilon_1$ then

$$(7.14) \qquad\qquad \mathbf{U}_{0,i_2,i_3}^{(1)} = \frac{\epsilon_2}{\epsilon_1}(\mathbf{n} \cdot \mathbf{U}_{0,i_2,i_3}^{(2)})\mathbf{n} + \sum_{m=1}^{2} \left(\boldsymbol{\tau}_m \cdot \mathbf{U}_{0,i_2,i_3}^{(2)}\right)\boldsymbol{\tau}_m.$$

A fourth-order accurate approximation will use two ghost lines on each side of the interface. The values at the ghost points are determined using fourth-order accurate approximations to the interface conditions for the first and second derivatives,

$$(7.15) \qquad [\epsilon \mathbf{n} \cdot \Delta_{4h} \mathbf{U_i}^{(k)}/(\epsilon\mu)]_{\mathcal{I}} = 0, \qquad [\boldsymbol{\tau}_m \cdot \Delta_{4h} \mathbf{U_i}^{(k)}/(\mu\epsilon)]_{\mathcal{I}} = 0,$$

$$(7.16) \qquad [\nabla_{4h} \cdot (\mathbf{U_i}^{(k)})]_{\mathcal{I}} = 0, \qquad [\mu^{-1}\boldsymbol{\tau}_m \cdot \nabla_{4h} \times \mathbf{U_i}^{(k)}]_{\mathcal{I}} = 0,$$

together with second-order accurate approximations to the interface conditions for the third and fourth derivatives,

$$(7.17) \qquad [(\nabla \cdot \Delta)_{2h}(\mathbf{U_i}^{(k)})]_{\mathcal{I}} = 0, \qquad [\mu^{-1}\boldsymbol{\tau}_m \cdot (\nabla \times \Delta)_{2h}\mathbf{U_i}^{(k)}/(\epsilon\mu)]_{\mathcal{I}} = 0,$$

$$(7.18) \qquad [\epsilon \mathbf{n} \cdot (\Delta^2)_{2h}\mathbf{U_i}^{(k)}/(\epsilon\mu)^2]_{\mathcal{I}} = 0, \qquad [\boldsymbol{\tau}_m \cdot (\Delta^2)_{2h}\mathbf{U_i}^{(k)}/(\epsilon\mu)^2]_{\mathcal{I}} = 0.$$

The fourth-order approximation will also impose equations (7.13). The accuracy and stability of these conditions for a model problem is considered in section 8.

A complicating factor in applying these interface boundary conditions is that the discrete equations couple the unknown values of $\mathbf{U_i}^{(k)}$ at all ghost points on both sides of the interface. Therefore, the solution to these equations requires the solution of a system of equations with the number of unknowns proportional to the number of points on the interface. In practice, it has been found that these equations can be approximately solved using an iterative technique (see section 9.3 for further details).
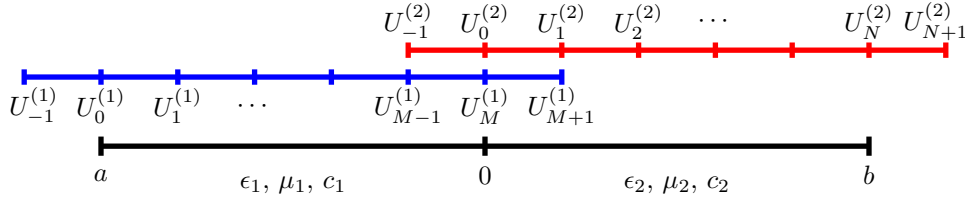

FIG. 3. *The overlapping grids for a one-dimensional material interface located at $x = 0$. Ghost points are introduced on the two grids at the interface.*

8. Analysis of the material interface conditions. The accuracy and stability of the centered boundary conditions for material interfaces is considered in this section. A semi-discrete one-dimensional model problem is studied using the Laplace transform in time and mode-analysis in space. Second-order accurate and fourth-order accurate interface conditions are analyzed.

A one-dimensional model problem for $u = u(x,t)$ and $v = v(x,t)$ on the interval $[a,b]$ with a material interface at $x = 0$, $a < x < b$, is

$$(8.1) \qquad \epsilon(x)u_{tt} = u_{xx}, \quad \epsilon(x)v_{tt} = v_{xx},$$

$$(8.2) \qquad [\epsilon u]_{\mathcal{I}} = 0, \qquad [v]_{\mathcal{I}} = 0,$$

$$(8.3) \qquad [u_x]_{\mathcal{I}} = 0, \qquad [v_x]_{\mathcal{I}} = 0,$$

where $\epsilon(x) = \epsilon_1$ for $x < 0$ and $\epsilon(x) = \epsilon_2$ for $x > 0$. The variable u represents the normal component of the field (say, E_x), while the variable v represents one of the tangential component of the field (say E_y). Note that for this model problem the equations for the normal and tangential components are decoupled.

Introduce a one-dimensional overlapping grid as shown in Figure 3. A (formally) second-order accurate semi-discrete approximation is

$$(8.4) \quad \epsilon_1 U_{tt}^{(1)} = D_+D_-U_j^{(1)}, \quad \epsilon_1 V_{tt}^{(1)} = D_+D_-V_j^{(1)}, \quad \text{for } j = M, M-1, M-2\ldots$$

$$(8.5) \quad \epsilon_2 U_{tt}^{(2)} = D_+D_-U_j^{(2)}, \quad \epsilon_2 V_{tt}^{(2)} = D_+D_-V_j^{(2)}, \quad \text{for } j = 0,1,2,\ldots$$

with interface conditions

$$(8.6) \qquad D_0 U_M^{(1)} = D_0 U_0^{(2)}, \qquad\qquad D_0 V_M^{(1)} = D_0 V_0^{(2)},$$

$$(8.7) \qquad D_+D_-U_M^{(1)} = D_+D_-U_0^{(2)}, \quad D_+D_-V_M^{(1)}/\epsilon_1 = D_+D_-V_0^{(2)}/\epsilon_2.$$

Here $U_i^{(k)}(t)$ and $V_i^{(k)}(t)$ denote the approximations to u and v on the grids while $D_+ = D_{+x}$, $D_- = D_{-x}$, and $D_0 = D_{0x}$ The grid points are denoted by $\mathbf{x}_i^{(k)}$. Approximations to the jump conditions $[u_{xx}]_{\mathcal{I}} = 0$ and $[v_{xx}/\epsilon]_{\mathcal{I}}$ have been imposed in place of (8.2); these follow from equations (8.1-8.2). The interface equations (8.6) and (8.7) can be solved for the values at the ghost points, $U_{M+1}^{(1)}$, $U_{-1}^{(2)}$ in terms of interior values,

$$(8.8) \qquad U_{M+1}^{(1)} = U_1^{(2)} + (U_M^{(1)} - U_0^{(2)}) = U_1^{(2)} + (\epsilon_2/\epsilon_1 - 1)U_0^{(2)}$$

$$(8.9) \qquad U_{-1}^{(2)} = U_{M-1}^{(1)} - (U_M^{(1)} - U_0^{(2)}) = U_{M-1}^{(1)} - (1 - \epsilon_1/\epsilon_2)U_M^{(1)}$$

$$(8.10) \qquad V_{M+1}^{(1)} = \frac{2\epsilon_1}{\epsilon_1 + \epsilon_2} V_1^{(2)} + \frac{\epsilon_2 - \epsilon_1}{\epsilon_1 + \epsilon_2}(2V_M^{(1)} - V_{M-1}^{(1)})$$

$$(8.11) \qquad V_{-1}^{(2)} = \frac{2\epsilon_2}{\epsilon_1 + \epsilon_2} V_{M-1}^{(1)} + \frac{\epsilon_1 - \epsilon_2}{\epsilon_1 + \epsilon_2}(2V_0^{(2)} - V_1^{(2)})$$

The interface boundary conditions have the useful property that when $\epsilon_1 = \epsilon_2$, the solution to the interface problem is the same as if there were no interface at all.

The stability of the discrete approximations to the interface problem will now be analyzed. A necessary condition for stability is the Godunov-Ryabenkii condition which requires that there be no solutions to the following eigenvalue problem for $\text{Re}(s) > 0$,

$$(8.12) \qquad \epsilon_1 s^2 W_j^{(1)} = D_+ D_- W_j^{(1)}, \qquad \text{for } j = M, M-1, M-2\ldots,$$

$$(8.13) \qquad \epsilon_2 s^2 W_j^{(2)} = D_+ D_- W_j^{(2)}, \qquad \text{for } j = 0, 1, 2, \ldots,$$

$$(8.14) \qquad D_0 W_M^{(1)} = D_0 W_0^{(2)}, \qquad (D_+ D_- W_M^{(1)})/\epsilon_1^\alpha = (D_+ D_- W_0^{(2)})/\epsilon_2^\alpha,$$

$$(8.15) \qquad \|W^{(1)}\|_h < \infty, \qquad \|W^{(2)}\|_h < \infty.$$

Here $\alpha = 0$ corresponds to the problem for the normal component $U_i^{(k)}$ while $\alpha = 1$ corresponds to the problem for the tangential component $V_i^{(k)}$. The discrete norms of the grid functions are defined from $\|W^{(1)}\|_h^2 = \sum_{j=-\infty}^{M} |W_j^{(1)}|^2 \, h$ and $\|W^{(2)}\|_h^2 = \sum_{j=0}^{\infty} |W_j^{(2)}|^2 \, h$. If this problem (8.12-8.15) were to have a solution, there would be a solution to equations (8.4-8.7) of the form $U_i^{(k)}(t) = e^{st} W_i^{(k)}$ that would grow arbitrarily fast in time as $h \to 0$, and the scheme would not be stable.

LEMMA 8.1. *The second-order accurate interface approximation (8.4-8.7) satisfies the Godunov-Ryabenkii condition.*

Proof. The solution to the eigenvalue problem (8.12-8.15) is of the form

$$W_j^{(1)} = A\kappa_1^{M-j}, \quad W_j^{(2)} = B\kappa_2^j,$$

where $\kappa_k = 1 + s_k/2 - \sqrt{s_k}\sqrt{1 + s_k/4}$ is a root of the characteristic equation $\kappa - 2 + \kappa^{-1} = s_k$, with $s_k = \epsilon_k s^2 h^2$, for $k = 1, 2$. The branch of the square root is taken so that $|\kappa_1| < 1$ and $|\kappa_2| < 1$ for $\text{Re}(s) > 0$. Applying the interface conditions (8.8) and (8.9) implies

$$A(\kappa_1^{-1} - \kappa_1) = B(\kappa_2 - \kappa_2^{-1}),$$

$$A(\kappa_1^{-1} - 2 + \kappa_1)/\epsilon_1^\alpha = B(\kappa_2 - 2 + \kappa_2^{-1})/\epsilon_2^\alpha.$$

For the case $\alpha = 0$ the determinant condition for nontrivial solutions is

$$(\kappa_1^{-1} - \kappa_1)(\kappa_2 - 2 + \kappa_2^{-1}) = (\kappa_2 - \kappa_2^{-1})(\kappa_1^{-1} - 2 + \kappa_1),$$

which simplifies to $\kappa_1 \kappa_2 = 1$. This contradicts the fact that $|\kappa_1 \kappa_2| < 1$ and thus there can be no non-trivial solutions. For $\alpha = 1$ it follows that $A = B$ and for a nontrivial solution, $-(\kappa_1 - \kappa_1^{-1}) = \kappa_2 - \kappa_2^{-1}$. From the definitions of κ_1 and κ_2 it follows that $\sqrt{s_1}\sqrt{1 + s_1/4} = -\sqrt{s_2}\sqrt{1 + s_2/4}$. The solution to the last equation is

$s_1 = -s_2 - 4$ (the other possible solution $s_1 = s_2$ is on the wrong branch of the square root) which implies $s = \pm i/(h\sqrt{\epsilon_1 + \epsilon_2})$. This contradicts the assumption that $Re(s) > 0$ and thus there are no nontrivial solutions for $\alpha = 1$. It thus follows that the Godunov-Ryabenkii condition is satisfied $\square$.

The accuracy of the approximation can be determined by examining the problem for the error, $E_i^{(k)} = U_i^{(k)} - u(\mathbf{x}_i^{(k)}, t)$,

$$\epsilon_1 s^2 E_j^{(1)} = D_+ D_- E_j^{(1)} + h^2 F_1, \qquad \text{for } j = M, M-1, M-2\ldots,$$
$$\epsilon_2 s^2 E_j^{(2)} = D_+ D_- E_j^{(2)} + h^2 F_2, \qquad \text{for } j = 0, 1, 2, \ldots,$$
$$D_0 E_M^{(1)} - D_0 E_0^{(2)} = h^2 G_1, \qquad (D_+ D_- E_M^{(1)})/\epsilon_1^\alpha - (D_+ D_- E_0^{(2)})/\epsilon_2^\alpha = h^2 G_2,$$

where the terms $h^2 F_1$, $h^2 F_2$, $h^2 G_1$ and $h^2 G_2$ are the truncation errors. In the usual manner (for example, see [14]), by subtracting out a solution to the Cauchy problem it may be assumed that $F_1 = F_2 = 0$. The solution to the error equations is then of the form

$$E_j^{(1)} = A\kappa_1^{M-j}, \quad E_j^{(2)} = B\kappa_2^j$$

and applying the interface conditions gives the equations for A and B,

$$\begin{bmatrix} (\kappa_1^{-1} - \kappa_1)/(2h) & -(\kappa_2 - \kappa_2^{-1})/(2h) \\ \epsilon_1^{1-\alpha} s^2 & -\epsilon_2^{1-\alpha} s^2 \end{bmatrix} \begin{bmatrix} A \\ B \end{bmatrix} = \begin{bmatrix} h^2 G_1 \\ h^2 G_2 \end{bmatrix}.$$

Using $\kappa_k - \kappa_k^{-1} = -2\sqrt{s_k}\sqrt{1 + s_k/4}$, it follows that

$$A = \frac{\epsilon_1^{1-\alpha} s G_1 + \epsilon_2^{1/2} G_2}{\epsilon_1^{1-\alpha}(\epsilon_1^{1/2} + \epsilon_2^{1/2}) s^2} h^2 + O(h^4), \quad B = \frac{\epsilon_1^{1-\alpha} s G_1 - \epsilon_1^{1/2} G_2}{\epsilon_1^{1-\alpha}(\epsilon_1^{1/2} + \epsilon_2^{1/2}) s^2} h^2 + O(h^4).$$

Therefore the solution to the semi-discrete problem is second-order accurate.

Now consider the fourth-order accurate approximation

$$(8.16) \qquad \epsilon_1 U_{tt}^{(1)} = D_+ D_- (1 - \tfrac{h^2}{12} D_+ D_-) U_j^{(1)}, \quad \text{for } j = M, M-1, M-2\ldots,$$

$$(8.17) \qquad \epsilon_2 U_{tt}^{(2)} = D_+ D_- (1 - \tfrac{h^2}{12} D_+ D_-) U_j^{(2)}, \quad \text{for } j = 0, 1, 2, \ldots,$$

$$(8.18) \qquad D_0 (1 - \tfrac{h^2}{6} D_+ D_-) U_M^{(1)} = D_0 (1 - \tfrac{h^2}{6} D_+ D_-) U_0^{(2)},$$

$$(8.19) \qquad D_+ D_- (1 - \tfrac{h^2}{12} D_+ D_-) U_M^{(1)}/\epsilon_1^\alpha = D_+ D_- (1 - \tfrac{h^2}{12} D_+ D_-) U_0^{(2)}/\epsilon_2^\alpha,$$

$$(8.20) \qquad D_0 D_+ D_- U_M^{(1)}/\epsilon_1 = D_0 D_+ D_- U_0^{(2)}/\epsilon_2,$$

$$(8.21) \qquad (D_+ D_-)^2 U_M^{(1)}/\epsilon_1^{1+\alpha} = (D_+ D_-)^2 U_0^{(2)}/\epsilon_2^{1+\alpha}.$$

where $\alpha = 0$ corresponds to the interface conditions for the normal component and $\alpha = 1$ the conditions for the tangential component. Two ghost points have been added to the grids on each side of the interface. Appropriate initial conditions are also required to complete the specification of the problem; their precise form is not germane to the following discussion. When $\epsilon_1 = \epsilon_2$, the solution to the interface problem reduces to the solution of the equations with no interface present since in this case $U_{M+m}^{(1)} = U_m^{(2)}$ and $U_{-m}^{(2)} = U_{M+m}^{(1)}$ for $m = 1, 2$.

The Godunov-Ryabenkii condition, necessary for the stability of solutions to these difference equations, requires that there be no solutions with $Re(s) > 0$ to the eigen-

value problem

$$\epsilon_1 s^2 W_j^{(1)} = D_+ D_- (1 - \tfrac{h^2}{12} D_+ D_-) W_j^{(1)}, \quad \text{for } j = M, M-1, M-2\ldots,$$

$$\epsilon_2 s^2 W_j^{(2)} = D_+ D_- (1 - \tfrac{h^2}{12} D_+ D_-) W_j^{(2)}, \quad \text{for } j = 0, 1, 2, \ldots,$$

$$D_0 (1 - \tfrac{h^2}{6} D_+ D_-) W_M^{(1)} = D_0 (1 - \tfrac{h^2}{6} D_+ D_-) W_0^{(2)},$$

$$D_+ D_- (1 - \tfrac{h^2}{12} D_+ D_-) W_M^{(1)} / \epsilon_1^\alpha = D_+ D_- (1 - \tfrac{h^2}{12} D_+ D_-) W_0^{(2)} / \epsilon_2^\alpha,$$

$$D_0 D_+ D_- W_M^{(1)} / \epsilon_1 = D_0 D_+ D_- W_0^{(2)} / \epsilon_2,$$

$$(D_+ D_-)^2 W_M^{(1)} / \epsilon_1^{1+\alpha} = (D_+ D_-)^2 W_0^{(2)} / \epsilon_2^{1+\alpha},$$

$$\|W^{(1)}\|_h < \infty, \qquad \|W^{(2)}\|_h < \infty.$$

LEMMA 8.2. *The fourth-order accurate interface approximation (8.16-8.21) satisfies the Godunov-Ryabenkii condition for $sh \ll 1$.*

Proof. For $\mathrm{Re}(s) > 0$ the bounded solutions may be written as

$$W_j^{(1)} = A_1 \kappa_1^{M-j} + B_1 \widetilde{\kappa}_1^{M-j}, \quad W_j^{(2)} = A_2 \kappa_2^j + B_2 \widetilde{\kappa}_2^j,$$

where κ_k are the roots approximating the solution to the continuous problem and $\widetilde{\kappa}_k$ are the spurious roots.[1] These are roots of the characteristic equation

$$(\kappa - 2 + \kappa^{-1})(1 - \tfrac{1}{12}(\kappa - 2 + \kappa^{-1})) = s_k,$$

where $s_k = \epsilon_k s^2 h^2$. In particular

$$\kappa_k = 1 + z_k/2 - \sqrt{z_k}\sqrt{1 + z_k/4}, \quad \widetilde{\kappa}_k = 1 + \widetilde{z}_k/2 - \sqrt{\widetilde{z}_k}\sqrt{1 + \widetilde{z}_k/4},$$

$$z_k = 6(1 - \sqrt{1 - s_k/3}), \qquad \widetilde{z}_k = 6(1 + \sqrt{1 - s_k/3}),$$

where the branch of the square root is chosen so that $|\kappa_k| < 1$ and $|\widetilde{\kappa}_k| < 1$ for $\mathrm{Re}(s) > 0$. Note that for $s_k = 3$ there is a double root $\kappa_k = \widetilde{\kappa}_k$ but this occurs when sh is order 1 and thus will not be considered. For $sh \ll 1$, the roots take the form

$$\kappa_k = 1 - \sqrt{\epsilon_k} sh + \epsilon_k (sh)^2/2 - (\sqrt{\epsilon_k} sh)^3/6 + (\sqrt{\epsilon_k} sh)^4/24 + O((sh)^5),$$

$$\widetilde{\kappa}_k = \frac{1}{7 + 4\sqrt{3}} + O(sh).$$

It can be seen that κ_k is a fourth-order approximation to $e^{-\sqrt{\epsilon_k} sh}$. Substitution of $W_j^{(1)}$ and $W_j^{(1)}$ into the four boundary conditions implies

$$(8.22) \qquad \begin{bmatrix} \mathcal{D}_1(\kappa_1) & \mathcal{D}_1(\widetilde{\kappa}_1) & \mathcal{D}_1(\kappa_2) & \mathcal{D}_1(\widetilde{\kappa}_2) \\ s_1/\epsilon_1^\alpha & s_1/\epsilon_1^\alpha & -s_2/\epsilon_2^\alpha & -s_2/\epsilon_2^\alpha \\ \mathcal{D}_3(\kappa_1)/\epsilon_1 & \mathcal{D}_3(\widetilde{\kappa}_1)/\epsilon_1 & \mathcal{D}_3(\kappa_2)/\epsilon_2 & \mathcal{D}_3(\widetilde{\kappa}_2)/\epsilon_2 \\ \mathcal{D}_4(\kappa_1)/\epsilon_1^{1+\alpha} & \mathcal{D}_4(\widetilde{\kappa}_1)/\epsilon_1^{1+\alpha} & -\mathcal{D}_4(\kappa_2)/\epsilon_2^{1+\alpha} & -\mathcal{D}_4(\widetilde{\kappa}_2)/\epsilon_2^{1+\alpha} \end{bmatrix} \begin{bmatrix} A_1 \\ B_1 \\ A_2 \\ B_2 \end{bmatrix} = \mathbf{0}$$

where $\mathcal{D}_1(\kappa) = \tfrac{1}{2}(\kappa - \kappa^{-1})(1 - \tfrac{1}{6}(\kappa - 2 + \kappa^{-1}))$, $\mathcal{D}_3(\kappa) = \tfrac{1}{2}(\kappa - \kappa^{-1})(\kappa - 2 + \kappa^{-1})$, and $\mathcal{D}_4(\kappa) = (\kappa - 2 + \kappa^{-1})^2$. Let $\mathcal{M}$ denote the matrix appearing in equation (8.22). Note that $\kappa_k - \kappa_k^{-1} = -2\sqrt{z_k}\sqrt{1 + z_k/4}$ and $\kappa_k - 2 + \kappa_k^{-1} = z_k$ which can be used to simplify the entries in $\mathcal{M}$. For stability there should be no values of s with $\mathrm{Re}(s) > 0$ when the determinant of $\mathcal{M}$ is zero. This condition is difficult to prove for general values of sh. For $sh \ll 1$, corresponding to the resolved modes in the discrete solution, the elements of the determinant can be expanded in powers of sh and one finds that for $sh \to 0$,

$$(8.23) \qquad \det(\mathcal{M}) \sim -2^9 3^3 \sqrt{3}(\epsilon_1^{-1/2} + \epsilon_2^{-1/2}) (sh)^3, \qquad\qquad \text{for } \alpha = 0,$$

$$(8.24) \qquad \det(\mathcal{M}) \sim -2^8 3^3 \sqrt{3}\frac{1}{\epsilon_1^2 \epsilon_2^2}(\epsilon_1^{1/2} + \epsilon_2^{1/2})(\epsilon_1 + \epsilon_2) (sh)^3, \quad \text{for } \alpha = 1.$$
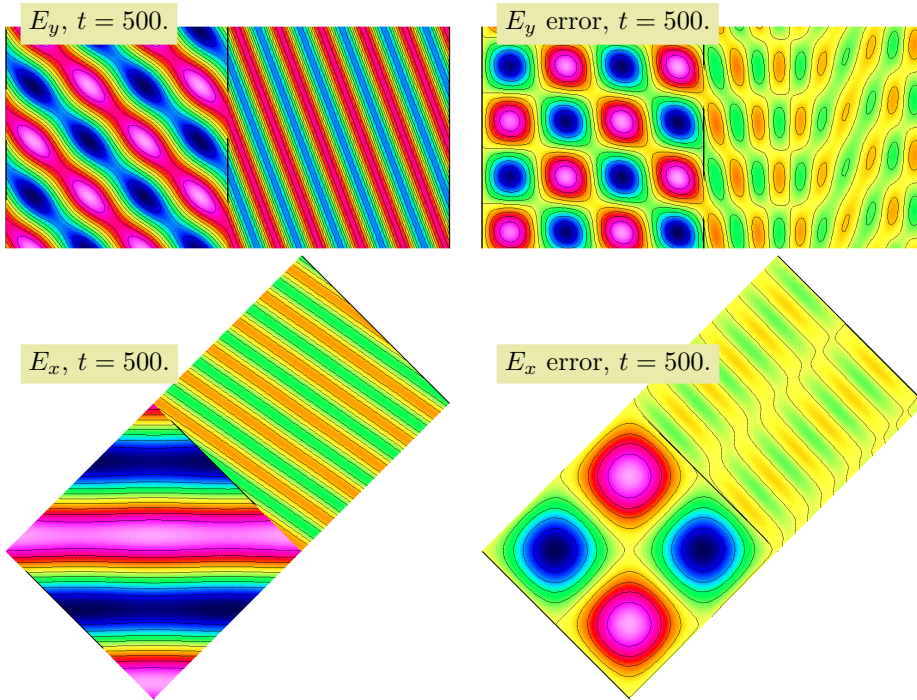
FIG. 4. *The reflection and transmission of a plane wave by a straight interface computed with the fourth-order accurate method. Top left: contours of E_y at $t = 500$. Top right: the error in E_y at $t = 500$ (the maximum error is .01). Bottom: the domain is rotated by 45°. Bottom left: contours of E_x at $t = 500$. Bottom right: the error in E_x at $t = 500$ (the maximum error is .05).*

Therefore there are no unstable modes for $sh \ll 1$ with $Re(s) > 0$. This proves the lemma $\square$.

The stability of the interface boundary conditions was investigated further by computing the reflection and transmission of an electromagnetic wave from a straight interface. The computational domain is the region $\Omega = [-1, 1] \times [0, 1]$, with the interface located at $x = 0$. A Cartesian grid, $\mathcal{G}_1$, with $N_1 \times M_1$ grid cells covers the left half of the domain, $\Omega_1 = [-1, 0] \times [0, 1]$, where the material properties are ϵ_1, and μ_1. Another Cartesian grid, $\mathcal{G}_2$, with $N_2 \times M_2$ grid cells covers the right half of the domain, $\Omega_2 = [0, 1] \times [0, 1]$, where the material properties are ϵ_2, and μ_2. The incident field was chosen to be $(E_x, E_y) = (-k_2, k_1)/|\mathbf{k}| \exp(2\pi i(\mathbf{k} \cdot \mathbf{x} - \omega t))$ where $\mathbf{k} = (k_1, k_2)$ and $\omega/|\mathbf{k}| = c_1$. The reflected and transmitted fields are easily determined [2]. The solution was evaluated using the fourth-order modified equation method (6.1) and the fourth-order accurate interface boundary conditions (7.15-7.18). See section 9.3 for further details of the implementation. Periodic boundary conditions were chosen at $y = 0$ and $y = 1$ and the exact solution was given as a boundary condition at $x = -1$ and $x = 1$. Figure 4 shows results for the case $\epsilon_1 = 1$, $\mu_1 = 1$ ($c_1 = 1$), $\epsilon_2 = 4$, $\mu_2 = 1$ ($c_2 = 1/2$), $\mathbf{k} = (2, 2)$, and $N_1 = M_1 = N_2 = M_2 = 80$. The solution was computed to time $t = 500$ (approximately $60,000$ time steps). The solution remained stable as evidenced by the smooth behaviour of the solution and error. Figure 4 shows similar results for a domain rotated by 45 degrees using $\mathbf{k} = (1, 1)$, $\epsilon_1 = 1$, $\mu_1 = 1$ ($c_1 = 1$), $\epsilon_2 = 16$, $\mu_2 = 1$ ($c_2 = 1/4$) and $N_1 = M_1 = N_2 = M_2 = 80$. The solution remained stable in this case as well.

For the long time non-dissipative calculations of Figure 4, the material interface conditions must be solved accurately to avoid a late time instability. More accuracy is required the larger the number of time steps. For accuracy reasons alone, only a few of iterations are needed. For the problem of scattering by a dielectric cylinder of section 10.3, when dissipation is added to the equations, only a few iterations are needed to solve the interface conditions since the dissipation suppresses this weak

---

[1]This form must be modified to use $j\kappa_k^j$ instead of $\widetilde{\kappa}^j$ when there is a double root, $\kappa_k = \widetilde{\kappa}_k$.

instability. If need arises the interface equations should be amenable to solution by a Krylov based method.

9. Implementation of the scheme. Some aspects of the implementation of the discrete approximations to the differential operators and boundary conditions will be considered in this section. The intent of these remarks is to give a basic outline of the implementation, a more detailed description is left for a future report. In typical cases the majority of grid points on an overlapping grid belong to Cartesian grids where the discrete approximations are straight-forward to implement. The Cartesian grid approximations are very fast to evaluate and use little memory. The majority of the programming effort, however, is concerned with implementing the approximations to the boundary conditions and material interface conditions on curvilinear grids.

9.1. Solving the PEC boundary conditions. The solution of the discrete approximations to the boundary conditions for a perfect electrical conductor are based upon the boundary conditions $\mathbf{n} \times \mathbf{E} = 0$ and $\nabla \cdot \mathbf{E} = 0$, together with the compatibility conditions (3.3). To simplify the implementation, some approximations are made that do not seem to affect the overall accuracy, as evidenced by the numerical results from section 10. The divergence of $\mathbf{E}$ can be written in general curvilinear coordinates as

$$\nabla \cdot \mathbf{E} = J^{-1} \sum_{m=1}^{d} \frac{\partial}{\partial r_m}(\mathbf{a}_m \cdot \mathbf{E}), \quad \mathbf{a}_m = J \nabla_{\mathbf{x}} r_m = J(\partial_x r_m, \partial_y r_m, \partial_z r_m) \ .$$

For a PEC boundary, corresponding to the parameter space line $r_1 = 0$, the boundary condition $\nabla \cdot \mathbf{E} = 0$ becomes a condition relating the r_1-derivative of $\mathbf{a}_1 \cdot \mathbf{E} = -J\|\nabla_{\mathbf{x}} r_1\|\mathbf{n} \cdot \mathbf{E}$ to tangential derivatives of the components $\mathbf{a}_2 \cdot \mathbf{E}_2$ and $\mathbf{a}_3 \cdot \mathbf{E}$, $\partial_{r_1}(\mathbf{a}_1 \cdot \mathbf{E}) = -\partial_{r_2}(\mathbf{a}_2 \cdot \mathbf{E}_2) - \partial_{r_3}(\mathbf{a}_3 \cdot \mathbf{E})$. For an orthogonal grid, $\mathbf{a}_2 \cdot \mathbf{E}(0, r_2, r_3) = 0$ and $\mathbf{a}_3 \cdot \mathbf{E}(0, r_2, r_3) = 0$ on the boundary since $\mathbf{a}_2$ and $\mathbf{a}_3$ are in the tangent plane. In addition, $\mathbf{a}_1 \cdot \mathbf{E}$ is (always) proportional to the normal component of $\mathbf{E}$, and thus the $\nabla \cdot \mathbf{E} = 0$ boundary condition reduces to a normal derivative of this component

$$J \ \nabla \cdot \mathbf{E} = \partial_{r_1}(\mathbf{a}_1 \cdot \mathbf{E}), \quad \text{for } r_1 = 0 \quad \text{(orthogonal grid)}.$$

For general grids $\mathbf{a}_2 \cdot \mathbf{E}_2$ and $\mathbf{a}_3 \cdot \mathbf{E}$ are not zero. A second-order accurate approximation to the boundary conditions at $i_1 = 0$ is

(9.1) $$\boldsymbol{\tau}_m \cdot \mathbf{U_i} = 0,$$

(9.2) $$D_{0,r_1}(\mathbf{a}_1 \cdot \mathbf{U_i}) = -D_{0,r_2}(\mathbf{a}_2 \cdot \mathbf{U_i}) - D_{0,r_3}(\mathbf{a}_3 \cdot \mathbf{U_i}),$$

(9.3) $$\boldsymbol{\tau}_m \cdot D_{+r} D_{-r} \mathbf{U_i} = 0, .$$

where $\boldsymbol{\tau}_m$, $m = 1, 2$ are tangent vectors to the boundary (there is only one in two dimensions). The equations (9.2-9.3) determine the solution on the ghost point, $\mathbf{U}_{-1,i_2,i_3}$. Equation (9.3) approximates the more accurate compatibility condition $\boldsymbol{\tau}_m \cdot \Delta \mathbf{E} = 0$. These equations can be solved without iteration since the terms appearing on the right hand side of equation (9.2) involve known values on the boundary once equation (9.1) is applied.

Let $D_{r_m}^{(4)} = D_{0,r_m}(1 - \frac{1}{12}\Delta r_1^2 D_{+,r_m} D_{-,r_m})$ denote the fourth-order accurate approximation to $\partial / \partial r_m$. A fourth-order accurate approximation to the boundary conditions at $i_1 = 0$ is

(9.4) $$\boldsymbol{\tau}_m \cdot \mathbf{U_i} = 0,$$

(9.5) $$D_{r_1}^{(4)}(\mathbf{a}_1 \cdot \mathbf{U})_{\mathbf{i}} = -D_{r_2}^{(4)}(\mathbf{a}_2 \cdot \mathbf{U_i}) - D_{r_3}^{(4)}(\mathbf{a}_3 \cdot \mathbf{U_i}),$$

(9.6) $$\boldsymbol{\tau}_m \cdot (\Delta_{4h} \mathbf{U_i}) = 0,$$

(9.7) $$D_{0,r_1}(\mathbf{a}_1 \cdot \Delta_{2h} \mathbf{U_i}) = -D_{0,r_2}(\mathbf{a}_2 \cdot \Delta_{2h} \mathbf{U_i}) - D_{0,r_3}(\mathbf{a}_3 \cdot \Delta_{2h} \mathbf{U_i}),$$

(9.8) $$(D_{+,r_1} D_{-,r_1})^2 (\boldsymbol{\tau}_m \cdot \mathbf{U_i}) = 0.$$

Equations (9.5-9.8) will determine the solution at the two ghost lines, $\mathbf{U}_{-1,i_2,i_3}$ and $\mathbf{U}_{-2,i_2,i_3}$. Condition (9.8) is an approximation to the more accurate compatibility condition $\Delta_{2h}^2 (\boldsymbol{\tau}_m \cdot \mathbf{U_i}) = 0$. Δ_{4h} is the fourth-order accurate FD4 approximation,

and Δ_{2h} is the second-order accurate FD2 approximation to the Laplacian as defined in section 5. Equations (9.6-9.7) couple the unknown values at the ghost points with neighbouring points. These equations can be solved by iterating on the unknown values using an appropriate initial guess, only one or two iterations are normally required.

9.2. Numerical dissipation. A high-order dissipation is added to the scheme to stabilize the approximation from weak, high-frequency (with respect to the grid), instabilities that may develop near interpolation points and boundaries. The most unstable modes tend to be the *plus-minus waves* that oscillate in sign from one grid point to the next. The appearance of an instability can be explained in the following way, (see Reyna [35] for a careful analysis for the scalar wave equation on an overlapping grid). Except for simple cases of a single Cartesian grid or multiple matching Cartesian grids, the discrete operator for the method, including interpolation and boundary conditions, will not be exactly symmetric. As a result it can be expected that some of the eigenvalues of the discrete system will have a non-zero imaginary part. It follows from lemma 5.1 that the corresponding eigenvectors will be unstable. Since the scheme is accurate, one can expect that the well resolved modes will have accurate eigenvalues. The most unstable modes are likely associated with high-frequency modes that are not well resolved on the grid. The high-order dissipation is added to suppress these unstable modes. The dissipation is particularly effective for modes that vary rapidly in space. By default the dissipation is always added to the method.

At the continuous level, the dissipation of the second-order wave equation takes the form $u_{tt} = c^2 \Delta u - \alpha \, h^{2p}(-\Delta)^p u_t$, where h is a measure of the local grid spacing. For the fourth-order accurate scheme a fourth-order dissipation with $p = 2$ is typically used,

$$(9.9) \qquad U_{\mathbf{i}}^{n+1} - 2U_{\mathbf{i}}^n + U_{\mathbf{i}}^{n-1} = (c\Delta t)^2 \Delta_{4h} U_{\mathbf{i}}^n + \frac{(c\Delta t)^4}{12}(\Delta^2)_{2h} U_{\mathbf{i}}^n$$
$$- \alpha_d (c\Delta t)^2 \sum_{m=1}^d (\Delta r_m)^4 (D_{+r_m} D_{-r_m})^2 (U_{\mathbf{i}}^n - U_{\mathbf{i}}^{n-1})/\Delta t.$$

The coefficient α_d is typically chosen to be about 1. The scheme remains fourth-order accurate provided $\alpha_d = O(1)$. The damping acts as a low pass filter, having little effect on the waves that are well resolved on the grid but rapidly damping the modes that are not resolved on the grid. It is also possible to use a sixth-order dissipation with the fourth order scheme, but this does not seem to provide any significant advantage.

9.3. Material interfaces. The boundary conditions for material interfaces have been implemented in two dimensions. Both second- and fourth-order accurate approximations have been developed; see sections 8 and 10.3 for some fourth-order accurate computations. The implementation is currently restricted to the case when the grids that meet at the interface have matching grids points (as shown, for example, in the grid in Figure 7). Currently only a simple iteration is used to solve the coupled interface equations. A more sophisticated solution scheme could be useful, but this option has not been investigated.

The solution of the fourth-order accurate approximations in two dimensions will be discussed here, the second-order accurate case is similar. Assume, as in section 7, that the interface corresponds to the line $i_1 = 0$, with the unknown ghost point values being $\mathbf{U}_{-m,i_2,i_3}^{(k)}$, for the ghost lines $m = 1, 2$, on the two sides of the interface, $k = 1, 2$. As a first step, the basic jump conditions (7.3–7.4) for the electric field are imposed. These conditions are used to assign the values of the electric field $\mathbf{U}_{0,i_2,i_3}^{(k)}$ for the side of the interface with the larger value of ϵ. The interface compatibility conditions are given by equations (7.15–7.18). The solution to these equations will determine the values at the ghost points on both sides of the interface. Approximations for Δ_{4h}, ∇_{4h} $(\nabla \cdot \Delta)_{2h}$ etc. are obtained with the mapping method (section 5). Three of the conditions (7.15,7.17,7.18) cause the equations to be coupled between adjacent points along the boundary, although on an orthogonal grid only the higher-order correction conditions (7.17,7.18) lead to coupling. At the start of the iteration the values on the

ghost points on both sides of the interface are given initial values by extrapolation. Then, at each step in the iteration, a small system of equations is solved at each point, $(0, i_2)$ along the boundary, for the 8 unknown values $\mathbf{U}^{(k)}_{-m, i_2, i_3}$, $m = 1, 2$, $k = 1, 2$ using the 8 equations (7.15–7.18). There will be 12 unknowns and 12 equations in three dimensions. When solving these equations the values at adjacent points are kept fixed at their most recent values.

For the long time computations presented at the end of section 8, which included no dissipation, it was found necessary to solve the interface equations very accurately (approximately 30 iterations) to avoid the development of late time instabilities. With the addition of a small fourth-order dissipation the number of iterations can be reduced to just a few. For the computations presented in section 10.3, which included a small fourth-order dissipation, it was found sufficient to use only one or two iterations to approximately solve the interface equations.

9.4. Parallel implementation. The algorithms described here have been implemented in the computer code **mx**. The **mx** solver is implemented at a high level in C++. It is based upon the Overture class library [2]. Most of the numerically intensive kernels are written in Fortran77. The overhead in using C++ is found to be negligible for any reasonable size problem (see section 10.5). The computer code **mx** runs on both serial and distributed memory parallel computers.

In a distributed parallel computing environment, the grid functions on each component grid (representing the solution variables such as E_x, E_y, E_z, etc.) are represented as multi-dimensional arrays. These arrays can be distributed across one or more processors. The grid functions are implemented using parallel distributed arrays from the P++ array class library [34]. Each P++ array can be independently distributed across the available processors. The distributed array consists of a set of serial arrays, one serial array for each processor. Each serial array is a multi-dimensional array that can be operated on using array operations. The data from the serial array can also be passed to a Fortran function, for example. When running in parallel, the serial arrays contain extra ghost lines that hold copies of the data from the serial arrays on neighbouring processors. P++ is built on top of the Multiblock PARTI parallel communication library [40], which is used for ghost boundary updates and copying blocks of data between arrays with possibly different parallel distributions.

A special parallel overlapping grid interpolation routine has been developed for updating the points on grids that interpolate from other grids. Overlapping grid interpolation is based on a multi-dimensional tensor product Lagrange interpolant. In parallel, the Lagrange formula is evaluated on the processor that owns the data in the stencil (the donor points), the resulting sums are collected into a message and then sent to the processor that owns the interpolation points. There is at most one message that needs to be sent between any two processors. In this way, the number of messages and the size of the messages that need to be passed between processors is quite small.

Figure 5 shows some results from solving Maxwell's equations with the **mx** solver on a distributed memory Linux cluster (with 2.4 GHz Zeon processors). The equations are solved to fourth-order accuracy. In these examples the number of grid points remains fixed as the number of processors is increased. The figure compares two-dimensional results for a square with 1024^2 ($1.1e6$) grid points to that of a circle-in-channel overlapping grid with $3.8e6$ grid points. The parallel scaling is very good in two dimensions for these problems since the number of computational points is large compared to the number of points where communication is required. Also shown are three-dimensional results for a box with 256^3 ($1.78e7$) grid points compared to a grid for a pill-box with about $3.2e6$ grid points (the pill-box appears in Figure 10). In the three-dimensional cases, there are relatively many more points where communication is required since for N^3 grid points in three-dimensions there are $O(N^2)$ points on the inter-processor boundaries. The parallel scaling is still reasonable with the results for the overlapping grid being comparable to that for the box.
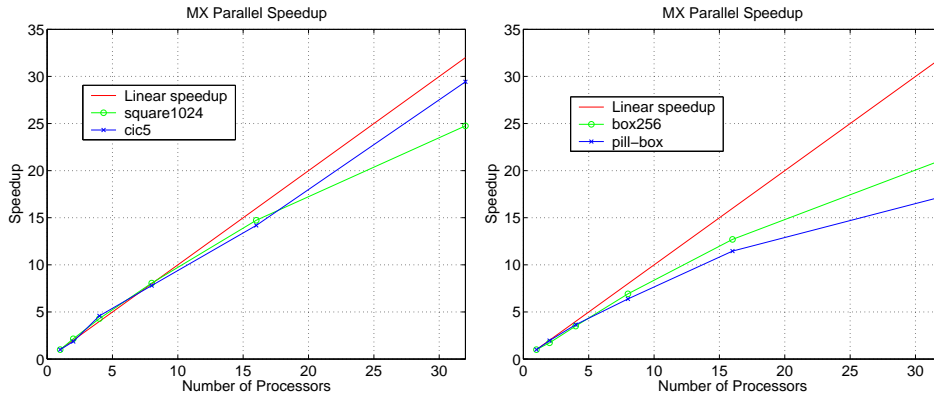
---

[2]http://www.llnl.gov/CASC/Overture.html

FIG. 5. *Strong scaling parallel results for the fourth-order accurate Maxwell solver. Left: speedup for a square with 1024^2 (1.1e6) points compared to a two-dimensional circle-in-a-channel grid with 3.8e6 grid points. Right: speedup for a box with 256^3 (1.78e7) grid points, compared to a pill-box grid with 3.2e6 grid points. Computations were performed on a Linux cluster.*

10. Numerical results. Numerical results will now be presented that demonstrate the accuracy and efficiency of the fourth order accurate version of the scheme. The scheme has also been verified on a number of other problems including the scattering of a plane wave by a two-dimensional cylinder and the computation of eigenmodes of a three-dimensional cylindrical cavity.

10.1. The method of analytic solutions. The *method of analytic solutions* is an extremely useful technique for constructing exact solutions to check the accuracy of a computer program. This method, also sometimes known as the *method of manufactured solutions* [36], or *twilight-zone forcing* [3] adds forcing functions to the governing equations and boundary conditions. These forcing functions are determined so that some given functions, $\mathbf{E}^{\text{true}}(\mathbf{x}, t)$, will be the exact solution to the forced equations. With this approach, the error in the discrete solution can be easily determined. Two common choices for exact solutions are low degree polynomials or trigonometric functions. The polynomial solutions are useful for checking that the fourth-order scheme can exactly solve a problem on a Cartesian grid, or overlapping Cartesian grids, when the degree of the polynomials is less than or equal to four. The trigonometric functions will be used in the convergence results given in this section. The exact solutions are chosen to be divergence free. In two- and three dimensions the functions are

$$(E_x^{\text{true}}, E_y^{\text{true}}, H_z^{\text{true}}) = \left(\tfrac{1}{2}c_xc_y, \tfrac{1}{2}s_xs_y, c_xs_y\right)\cos(\pi t),$$

$$(E_x^{\text{true}}, E_y^{\text{true}}, E_z^{\text{true}}) = \left(c_xc_yc_z, \tfrac{1}{2}s_xs_yc_z, \tfrac{1}{2}s_xc_ys_z\right)\cos(\pi t),$$

where $c_x = \cos(\pi x)$, $s_y = \sin(\pi x)$, etc. Define the error in the discrete approximation $U_{\mathbf{i}}^n$ to E_x at a given time t^n by

$$(10.1) \qquad\qquad e_{\mathbf{i}}^{E_x} = U_{\mathbf{i}}^n - E_x^{\text{true}}(\mathbf{x_i}, t^n) \ ,$$

with similar definitions for $e_{\mathbf{i}}^{E_y}$, $e_{\mathbf{i}}^{E_z}$ and $e_{\mathbf{i}}^{H_z}$ Define the discrete max-norm by

$$(10.2) \qquad\qquad \|U_{\mathbf{i}}^n\|_\infty = \max_{\mathbf{i}} |U_{\mathbf{i}}^n| \ ,$$

where the maximum is taken over all valid points in the overlapping grid.

Table (2) shows convergence results for a two-dimensional cylinder in a channel. The coarse grid, $\mathcal{G}_1$, for this case consists of a Cartesian grid for the square $[-2, 2]^2$ with 61×61 grid points, and an annular grid centered at the origin with inner radius $\frac{1}{2}$, outer radius $\frac{3}{4}$ and containing 81×5 grid points. The grids $\mathcal{G}_2$ and $\mathcal{G}_4$ are, respectively, two and four times finer in each direction. PEC boundary conditions are taken on all

boundaries. The results in the table show that the solution is converging at a rate close to 4 in the maximum norm. The non-dimensionalized divergence in $\mathbf{E}$, defined as $\delta_{\mathbf{E}} = \|\nabla \cdot \mathbf{E}\|_\infty / \|\nabla \mathbf{E}\|_\infty$, is small and also converging at a rate close to 4. The convergence rate σ was estimated by assuming an error of the form $E = Ch^\sigma$ and making a least squares fit for σ to the equation $\log(E) = \sigma \, \log(h) + \log(C)$.

grid	$\|\mathrm{e}^{E_x}\|_\infty$	$\|\mathrm{e}^{E_y}\|_\infty$	$\|\mathrm{e}^{H_z}\|_\infty$	$\delta_{\mathbf{E}}$
$\mathcal{G}_1$	$9.1e{-}5$	$6.4e{-}5$	$1.3e{-}4$	$1.7e{-}4$
$\mathcal{G}_2$	$4.2e{-}6$	$4.5e{-}6$	$8.1e{-}6$	$1.1e{-}5$
$\mathcal{G}_4$	$2.2e{-}7$	$2.9e{-}7$	$5.1e{-}7$	$7.8e{-}7$
rate σ	4.40	3.93	4.02	3.94

TABLE 1

Convergence rates for a two-dimensional cylinder in a channel grid. The maximum errors in E_x, E_y, H_z and $\delta_{\mathbf{E}} = \|\nabla \cdot \mathbf{E}\|_\infty / \|\nabla \mathbf{E}\|_\infty$ are shown at $t = 1$ for a trigonometric exact solution. The estimated convergence rate, $E \propto h^\sigma$, is also indicated.

Table (2) shows convergence results for solutions computed on a sphere in a box domain. The coarse grid, $\mathcal{G}_1$, in this case consists of three grids. A Cartesian grid covers the cube $[-2, 2]^3$ with 41^3 grid points. The sphere of radius $\frac{1}{2}$ is covered with two overlapping orthographic patches, each with $33 \times 33 \times 13$ grid points. The grids $\mathcal{G}_2$ and $\mathcal{G}_4$ are, respectively, two and four times finer in each direction. The fine grid $\mathcal{G}_4$ has about 6.4 million grid points. PEC boundary conditions are taken on all boundaries. The results in the table show the maximum errors and estimated convergence rates. The convergence rates for the errors in $\mathbf{E}$ are close to 4. The convergence rate for $\delta_{\mathbf{E}}$ is approximately 3.5 which is still reasonable considering that this quantity is derived from derivatives of the computed variables.

grid	$\|\mathrm{e}^{E_x}\|_\infty$	$\|\mathrm{e}^{E_y}\|_\infty$	$\|\mathrm{e}^{E_z}\|_\infty$	$\delta_{\mathbf{E}}$
$\mathcal{G}_1$	$1.1e{-}3$	$6.0e{-}4$	$1.4e{-}3$	$3.0e{-}3$
$\mathcal{G}_2$	$4.8e{-}5$	$1.9e{-}5$	$6.0e{-}5$	$2.1e{-}4$
$\mathcal{G}_4$	$3.7e{-}6$	$1.6e{-}6$	$4.6e{-}6$	$2.4e{-}5$
rate σ	4.12	4.26	4.11	3.47

TABLE 2

Convergence rates for a three dimensional sphere in a box domain. The maximum errors in E_x, E_y, E_z and the non-dimensionalized divergence $\delta_{\mathbf{E}}$ are shown at $t = 1$ for a trigonometric exact solution. The estimated convergence rate, $E \propto h^\sigma$, is also indicated.
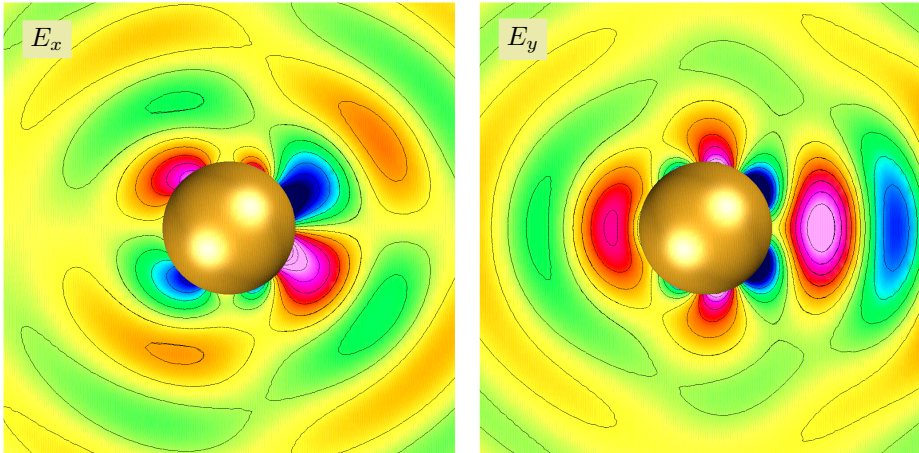

FIG. 6. *Scattering of a plane wave by a perfectly conducting sphere. The scattered fields for E_x and E_y are shown.*

10.2. Scattering by a PEC sphere. The scattering of an incident plane wave $\mathbf{E}^I = \left(e^{i(kx-\omega t)}, 0, 0\right)$ by a sphere of radius a is considered. The exact Mie series solution is well known [42]. The given incident field can be subtracted out, leaving the solution to the scattered field to be determined. A PEC boundary condition is imposed on the surface of the sphere, taking into account the incident field that has been removed. The initial conditions are taken as the exact solution for the scattered field at times $t = -\Delta t$ and $t = 0$. The exact solution is imposed on the outer boundaries of the domain. The solution is integrated to time $t = 3$. The grids, $\mathcal{G}_1$, $\mathcal{G}_2$ and $\mathcal{G}_4$ used for the sphere in a box are the same as those described in section 10.1. Table 3 presents the maximum errors and estimated convergence rates. The computed values of $\mathbf{E}$ are converging at rates close to 4. Figure 6 shows the scattered field for an incident wave with $ka = \pi$.

grid	$\|e^{E_x}\|_\infty$	$\|e^{E_y}\|_\infty$	$\|e^{E_z}\|_\infty$	$\delta_{\mathbf{E}}$
$\mathcal{G}_1$	$1.3e{-}2$	$8.1e{-}3$	$6.7e{-}3$	$3.9e{-}3$
$\mathcal{G}_2$	$9.3e{-}4$	$5.8e{-}4$	$4.8e{-}4$	$4.2e{-}4$
$\mathcal{G}_4$	$6.2e{-}5$	$3.9e{-}5$	$3.2e{-}5$	$5.4e{-}5$
rate σ	3.86	3.86	3.85	3.09

TABLE 3

The maximum errors at $t = 3$ for the computation of a plane wave scattering from a perfectly conducting sphere.
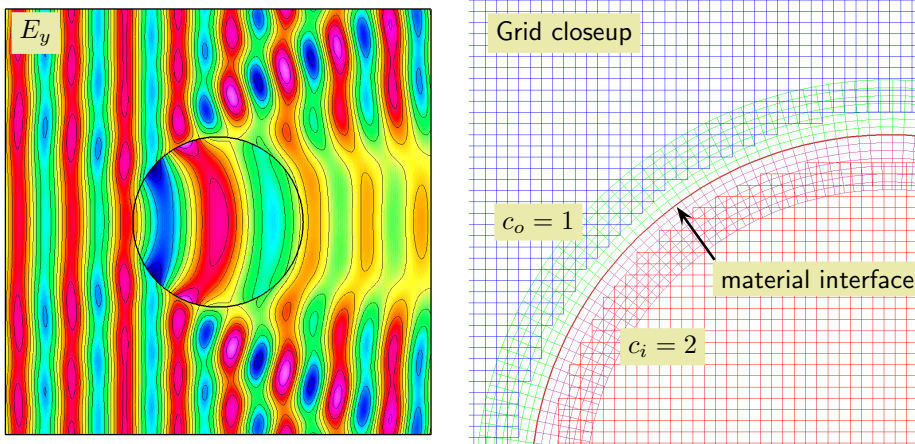

FIG. 7. *Scattering of a plane wave by a dielectric cylinder for $ka = 4\pi$, $c_o = 1$ and $c_i = 2$. The field component E_y is shown for the solution computed on grid $\mathcal{G}_4$. A closeup of the grid $\mathcal{G}_2$ near the interface is shown.*

10.3. Scattering of a plane wave by a dielectric cylinder. The two-dimensional computation of a plane wave hitting a dielectric (insulating) cylindrical disk possessing different material properties is used to test the accuracy of the material interface conditions presented in section 7. Consider a plane wave, $(E_x^I, E_y^I, H_z^I) = (0, \frac{\omega}{k} e^{i(kx-\omega t)}, e^{i(kx-\omega t)})$, incident upon a dielectric cylinder of radius a. Let ϵ_i be the electric permittivity for the region interior to the cylinder, ϵ_o the electric permittivity for the region outside the cylinder and $m = \sqrt{\epsilon_i/\epsilon_o} = c_o/c_i$ the relative index of refraction for the dielectric. (The magnetic permeability μ is assumed to be the same in both materials). The solution for the magnetic field in terms of the incident, scattered field and dielectric field is known as a series solution, see Balanis [2] or van de Hulst [42]. A closeup of the grid used in this computation is shown in Figure 7. The coarse grid, $\mathcal{G}_1$, for this domain consists of four component grids. A Cartesian grid covers the domain $[-1, 1]^2$ with 81×81 grid points. An annular grid of inner radius $a = \frac{1}{2}$, radial width .0875 covers the region immediately adjacent and exterior to the circle of radius $\frac{1}{2}$, centered at the origin. A second annular grid with the same radial

width and grid spacing covers the region just inside the circle and a second Cartesian grid lies in the central region. The refined versions of the grids are $\mathcal{G}_2$ and $\mathcal{G}_4$. The width of the annular grids are decreased by the same factor of 2 as the grids are refined so that there remain 6 grid points in the radial direction. The initial conditions at $t = 0$ and $t = -\Delta t$ are taken as the exact solution. The boundary condition on the outer boundaries is also taken as the exact solution.

Table 4 shows convergence results for the scattering of a plane wave by the dielectric cylinder for an incident wave number of $ka = 4\pi$ with $c_o = 1$ and $c_i = 2$. The fourth-order accuracy of the method is evident. The E_y component of the computed solution is shown in Figure 7. Note that the tangential component of the field is continuous at the interface but there is a jump in the normal component.

grid	$\|e^{E_x}\|_\infty$	$\|e^{E_y}\|_\infty$	$\|e^{H_z}\|_\infty$	$\delta_{\mathbf{E}}$
$\mathcal{G}_1$	$1.4e{-}1$	$2.9e{-}1$	$3.0e{-}1$	$6.7e{-}2$
$\mathcal{G}_2$	$1.0e{-}2$	$2.1e{-}2$	$2.2e{-}2$	$4.5e{-}3$
$\mathcal{G}_4$	$6.8e{-}4$	$1.4e{-}3$	$1.4e{-}3$	$2.9e{-}4$
rate σ	3.86	3.87	3.88	3.92

TABLE 4

Maximum errors at $t = 1$ in computing the scattering of a plane wave by a dielectric cylinder. The incident wave number was $ka = 4\pi$, with $\epsilon = 1/4$ inside the cylinder and $\epsilon = 1$ in the region exterior to the cylinder.

10.4. Computing eigenvalues of a disk and an L-shaped domain. The main focus of this paper has been on the solution of the time domain equations. In this section the computation of the frequency domain eigenvalues and eigenvectors will be briefly considered. Of particular interest will be the behaviour of the scheme in computing approximations to the highly singular solutions of a problem with a re-entrant corner.

The eigenvalue problem for Maxwell's equations is posed as

$$(10.3) \qquad\qquad -\Delta\mathbf{E} = \lambda\mathbf{E} \qquad\qquad \mathbf{x} \in \Omega,$$

$$(10.4) \qquad\qquad \mathbf{n} \times \mathbf{E} = 0, \quad \nabla \cdot \mathbf{E} = 0 \qquad \mathbf{x} \in \partial\Omega.$$

This formulation is sometimes called the "regularized" eigenvalue problem [18, 8] since the operator $\nabla \times \nabla$ has been replaced by the more *regular* operator $-\Delta$. This problem is discretized following the approximations and boundary conditions given in section 9, resulting in the generalized matrix eigenvalue problem $Ax = \lambda Mx$. The smallest eigenvalues of this system are determined using ARPACK [31]. Note that the eigenvalue problem (10.3-10.4) admits solutions with non-zero $\nabla \cdot \mathbf{E}$ (corresponding to the Dirichlet eigenvalues of the $-\Delta$ operator). These eigenvalues are removed as a post-processing step. Alternatively the original formulation (10.3-10.4) can be altered to eliminate these eigenvalues [17].

As a first example, consider the computation of the eigenvalues for the domain consisting of the unit disk, $\Omega = \{\mathbf{x} \in \mathbb{R}^2 \mid |\mathbf{x}| \leq 1\}$. The exact eigenvalues and eigenvectors for this problem are easily determined. The coarse grid, $\mathcal{G}_1$, for this case consists of a Cartesian grid for the square $[-.7, .7]^2$ with 25×25 grid points, and an annular grid centered at the origin with inner radius $\frac{3}{4}$, outer radius 1 and containing 61×7 grid points. Grids $\mathcal{G}_2$ and $\mathcal{G}_4$ have two and four times as many points in each direction. Figure 8 shows the coarse grid $\mathcal{G}_1$, the E_y component of the eigenvector for the smallest eigenvalue and the relative errors in the first five eigenvalues for the three different grids. The relative error is defined as the difference between the computed value and true value, divided by the true value. It is seen that the eigenvalues are computed very accurately with the values converging at a rate close to fourth-order.

As a second problem, the eigenvalues will be computed for the L-shaped domain $\Omega = [-1, 1]^2 - [-1, 0]^2$. This problem is quite difficult due to the highly singular nature of some of the eigenfunctions. The eigenfunction corresponding to the smallest eigenvalue, for example, becomes unbounded at the corner. It is known [8] that many
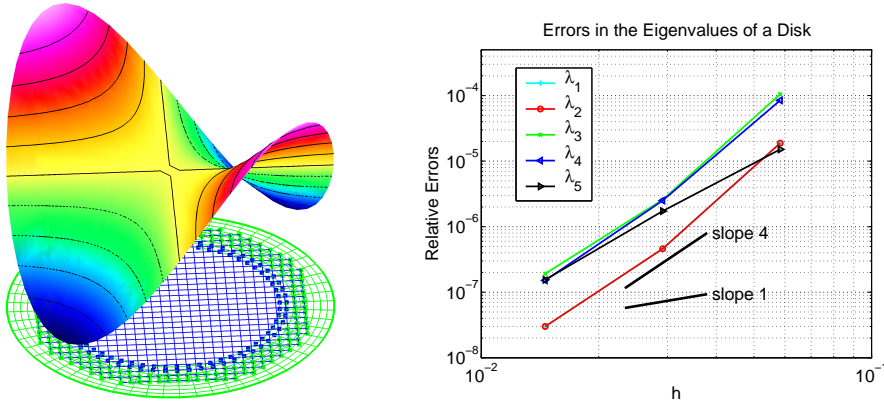
Fig. 8. *Solving the eigenvalue problem for the unit disk. Left: the coarse grid and the component E_y of the eigenvector for the smallest eigenvalue. Right: the relative errors in the smallest five eigenvalues for three different grid spacings.*

straight-forward finite difference and finite element approximations to the eigenvalue problem for a problem with a re-entrant corner will fail to approximate some of the singular eigenfunctions (those that become unbounded), and the corresponding eigenvalues will be missing entirely from the discretized equations. There are a number of proposed fixes to this problem including adding new degrees of freedom based on singular functions [8] or the use of a weighted regularization [5]. Note that both of these latter approaches could likely be adapted to the current discretization if so desired. The use of edge elements [33] and a sufficiently fine grid will not have these difficulties.

For the case here using overlapping grids, the corner problem will be dealt with by introducing a domain with a slightly rounded corner as shown in Figure 9. The radius of curvature of the rounded corner can be made as small as desired, given a sufficiently fine grid. This use of smooth boundary approximations to corners with large opening angles is one that the author generally recommends for other classes of problems as well. The coarse grid, $\mathcal{G}_1$, for the L-shaped domain consists of a total of six grids. There are three Cartesian grids for the three square domains $[-1, 0] \times [0, 1]$, $[0, 1]^2$, and $[0, 1] \times [-1, 0]$, each with 41×41 points. A small boundary fitted grid with 64×14 points is added to define a smooth rounded corner. Two additional nested refinement grids with 80×17 and 100×21 are added to this boundary fitted grid (see Figure 9). The boundary fitted grid is defined by an analytic function involving the logarithm of hyperbolic cosine functions [19]. Finer grids $\mathcal{G}_2$, $\mathcal{G}_4$ and $\mathcal{G}_6$ have two, four and six times as many points in each direction.

Figure 9 shows the relative errors in computing the first 5 of the smallest eigenvalues for the L-shaped domain. The coarse grid $\mathcal{G}_1$ is shown along with the E_x component of the eigenvector corresponding to the smallest eigenvalue. The eigenvalues for L-shaped domain correspond to the eigenvalues of the Neumann problem for the $-\Delta$ operator and have been computed very accurately[3], see Table 5. The relative errors shown in the figure and table are for the computed eigenvalues of the rounded domain compared to these accurate values for the domain with a sharp corner. The results from 9 indicate that all the smallest eigenvalues can be computed with reasonable accuracy. The convergence rates are between first and second-order accurate rather than fourth-order. This might be expected since the solutions and gradients are very large and not fully resolved. The eigenvalues of the rounded domain will also be slightly different from the domain with a sharp corner. It may be possible to improve the convergence rates by a more careful choice of grid or by incorporating knowledge of the singularity, following the approaches mentioned earlier.

The numerical values of the computed eigenvalues for the rounded corner are compared to the "exact" values for a sharp corner in Table 5. Note that the imaginary

---

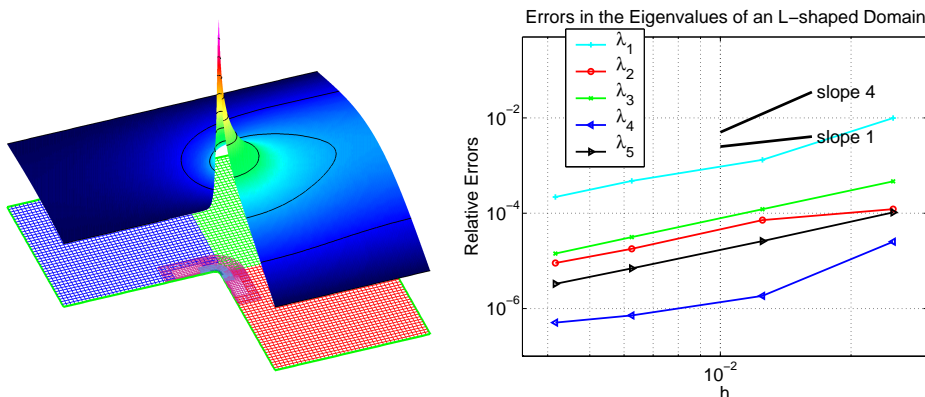[3] www.maths.univ-rennes1.fr/~dauge/benchmax.html

FIG. 9. *Solving the eigenvalue problem for an L-shaped domain. Left: the coarse grid $\mathcal{G}_1$ and the component E_x of the eigenvector for the smallest eigenvalue. The re-entrant corner is rounded off slightly and refined. Right: the relative errors in the smallest five eigenvalues for three different grid spacings.*

part of these computed eigenvalues are all found to be zero (to double precision accuracy). The matrix system $Ax = \lambda M x$ for the generalized eigenvalue problem will not in general be completely symmetric on an overlapping grid and thus there may be some eigenvalues with an imaginary part. It is expected that some high-frequency eigenvalues will have an imaginary part; these will correspond to the weakly unstable modes for the time-dependent problem. A high-order dissipation is added to the time domain algorithm to remove this instability (discussed in section 9.2).

	Computed	"exact"	Rel-err
λ_1	$(1.4903, 0.0)$	1.47562182	$9.93\mathrm{e}{-03}$
λ_2	$(3.5345, 0.0)$	3.53403137	$1.22\mathrm{e}{-04}$
λ_3	$(9.8650, 0.0)$	9.86960440	$4.67\mathrm{e}{-04}$
λ_4	$(9.8699, 0.0)$	9.86960440	$2.53\mathrm{e}{-05}$
λ_5	$(11.391, 0.0)$	11.3894794	$1.04\mathrm{e}{-04}$

TABLE 5

Real and imaginary parts, $(\mathrm{Re}(\lambda), \Im(\lambda))$, of the computed eigenvalues for the L-shaped domain with a rounded corner compared, the "exact" values for a sharp corner and the relative errors. Results are for the coarse grid $\mathcal{G}_1$.

10.5. Serial performance and memory usage. The performance of the **mx** solver on two problems, one two-dimensional and one three-dimensional, is given in Table 6. The two-dimensional problem is for a circle in a channel grid. The three-dimensional problem considered the computation in the pill-pox geometry shown in Figure 10. The table indicates the amount of time that is spent in various parts of the code. In the two-dimensional case, close to 70% of the time is spent in the Fortran kernel that advances the solution on the interior points of the Cartesian grid. Advancing the solution on the curvilinear grids takes about 14% while applying the boundary conditions on all grids takes about 11%. These results show that the overall performance of the code is approaching that of a purely Cartesian grid solver, provided a sufficiently high percentage of the grids points are Cartesian grid points.

In three-dimensions, the advancement of the curvilinear grids takes the most time at about 48% with the Cartesian grids taking 28% and boundary conditions and interpolation taking a total of about 22%. In three-dimensions the cost of advancing the curvilinear grid with a fourth-order approximation is on the order of 10 times slower per grid point than for a Cartesian grid. As the grids are refined the percentage of Cartesian grid points will increase since the number of Cartesian grid points scales like N^3 while the number of curvilinear grids points grows like N^2 (assuming that the curvilinear boundary fitted grids retain a fixed number of grid points in the normal direction as the grids are refined). Thus for sufficiently fine grids in three-dimensions

it can be expected that the time will be dominated by the work done on Cartesian grids.

	2D cylinder		3D pill-box	
	s/step	%	s/step	%
advance Cartesian grids	1.24	71.4	4.23	28.2
advance curvilinear grids	.242	14.0	7.18	47.8
boundary conditions	.184	10.6	2.23	14.8
interpolation	.008	0.46	1.01	6.8
other	.056	3.4	0.35	2.4
total	1.73	100	15.0	100

TABLE 6

CPU time (in seconds) per step for various parts of the code and their percentage of the total CPU time per step. Results for the two-dimensional cylinder in a channel problem (3.8 million grid points) are given in the two left columns. Results for the three-dimensional pill-box problem (10.2 million grid points) are given in the two right-most columns. Computations were performed on a desktop with a 2.2 GHz Zeon processor.

Table 7 gives the computer memory usage of the **mx** code for solving Maxwell's equations, to fourth-order accuracy, on the three-dimensional pill-box example of Figure 10. The table indicates the amount of memory required in MBytes for a double precision (64 bit) computation and the number of double precision floating point numbers required per grid point, denoted by reals/point. The number of reals/point for this computation was about 12.6. Only the **E** field was computed in this case. About 18% of the memory was dedicated to the storage of the overlapping grid (grid metrics, masks etc.). To put these numbers in context, note that if the Cartesian grids were treated as general curvilinear grids then the storage of the Jacobian matrix $\partial \mathbf{x}/\partial \mathbf{r}$ on the entire grid would itself require 9 reals/point. The **mx** solver is therefore seen to be quite memory efficient.

Memory Usage, Pill-box Problem			
	Mbytes	reals/pt	%
Overlapping grid	175.	2.3	17.8
Grid functions	779.	10.0	79.4
Other	26.	0.3	2.8
Total	980.	12.6	100.0

TABLE 7

Memory usage for the three-dimensional pill-box problem solved in double precision with the fourth-order accurate approximation. The grid for this problem contained about 10.2 million grid points with about 4.2e5 interpolation points. The number of double precision floating point numbers required per grid point was about 12.6 (reals/pt). About 17.8% of the memory was dedicated to the storage of the overlapping grid (grid metrics, masks etc.).

11. Conclusions. A scheme has been presented for the solution of the time-dependent Maxwell equations in complex geometries. The approach uses overlapping grids with a typical grid consisting of one or more background Cartesian grids overlapping body fitted curvilinear grids. Maxwell's equations are solved as a second-order vector wave equation. A three-level time stepping scheme is used that can be used to generate methods of order 2, 4, 6 and higher. High-order accurate symmetric finite difference approximations to the generalized Laplace operator have been developed. These approximations are symmetric on arbitrary logically rectangular curvilinear grids. Implementations of these operators in two- and three dimensions for orders 2, 4, 6 and 8 were shown to give energy preserving results when solving Maxwell's equations on a square and a box with randomly perturbed grid points. High-order accurate centered boundary conditions for perfect electrical conductor (PEC) boundaries have been devised. High-order accurate centered boundary conditions were also developed for material interfaces that separate regions with constant values of the material properties. The interfaces were represented with overlapping grids, using
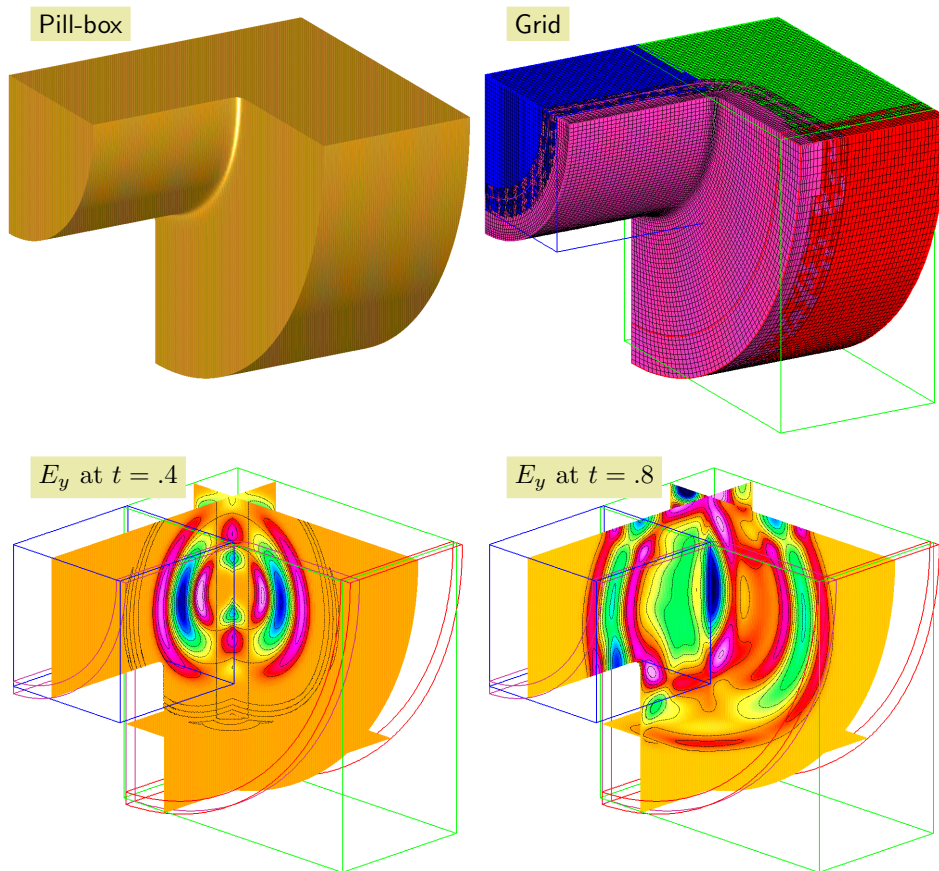
FIG. 10. *Propagation of a pulse in a pill-box cavity. Top left: the pill-box geometry. Top-right: the overlapping grid for the geometry (coarse grid version). Bottom: the electric field component E_y at two times. Contours of the field are plotted on planes that cut through the computational domain. The block-boundaries of the the grids are shown for reference.*

boundary fitted grids on each side of the interface. These centered boundary conditions are based on compatibility conditions derived from the governing equations. The stability and accuracy of the fourth-order accurate PEC approximations were analyzed for a model problem on a periodic strip. The stability of the material interface conditions were analyzed for a one-dimensional model problem for a second- and fourth-order approximation.

The approach has been implemented for computations on distributed memory multi-processor machines. The arrays holding the solution variables and grid metrics etc. on each component grid are distributed across one or more processors. An efficient parallel interpolation scheme has been developed for communicating the interpolation information where component grids overlap. Results from some parallel computations show that the algorithm scales well.

Numerical results for a number of two- and three-dimensional problems were used to verify the accuracy of the fourth-order accurate version of the method. The method of analytic solutions was used to generate *exact* solutions to the forced equations and verify the convergence rates. The scattering of a plane wave by a three-dimensional sphere was computed and shown to converge to fourth-order accuracy compared to the exact series solution. The material interface boundary conditions were verified to be fourth-order accurate for the scattering of a plane wave by a dielectric cylinder. The frequency domain eigenvalue problem was discretized using the fourth-order accurate approximations. Eigenmodes and eigenvalues of a two-dimensional disk and an L-shaped domain were determined. By rounding the sharp re-entrant corner of the L-shaped domain, the method was able to compute accurate approximations to the eigenvalues of the highly-singular eigenmodes. Statistics presented from some

representative computations showed that the method is very efficient in both speed and memory, especially when the overlapping grid for the domain consists mainly of Cartesian grid points. In that case the performance of the method can approach that of a Cartesian grid solver.

The **mx** Maxwell solver has been implemented using the Overture framework that has support for adaptive mesh refinement, moving grids and fast multigrid solvers for elliptic equations [22, 21]. These capabilities of Overture may be useful for future extensions of the the Maxwell solver. Far-field radiation conditions for boundaries of the computational domain that have been artificially truncated are an important consideration. The treatment of these far-field boundary conditions in conjunction with the present approach is left to a future publication. The general approach developed here can also be applied to other systems that take the form of a second-order wave equation, such as the equations of elasticity.

REFERENCES

[1] L. ANNÉ, P. JOLY, AND Q. H. TRAN, *Construction and analysis of higher order finite difference schemes for the 1d wave equation*, Computational Geosciences, 4 (2000), pp. 207–249.

[2] C. A. BALANIS, *Advanced Engineering Electromagnetics*, John Wiley & Sons, 1989.

[3] G. CHESSHIRE AND W. HENSHAW, *Composite overlapping meshes for the solution of partial differential equations*, J. Comput. Phys., 90 (1990), pp. 1–64.

[4] G. C. COHEN, *Higher-Order Numerical Methods for Transient Wave Equations*, Springer, New York, 2002.

[5] M. COSTABLE AND M. DAUGE, *Weighted regularization of Maxwell equations in polyhedral domains*, Numer. Math., 93 (2002), pp. 239–277.

[6] M. DABLAIN, *The application of high order differencing for the scalar wave equation*, Geophysics, 51 (1986), pp. 54–66.

[7] S. DEY AND R. MITTRA, *A locally conformal finite-difference time-domain (FDTD) algorithm for modeling three-dimensional perfectly conducting objects*, IEEE Microwave and Guided Wave Letters, 7 (1997), pp. 273–275.

[8] A.-S. B.-B. DHIA, C. HAZARD, AND S. LOHRENGEL, *A singular field method for the solution of Maxwell's equations in polyhedra domains*, SIAM J. Appl. Math., 59 (1999), pp. 2028–2024.

[9] A. DITKOWKSI, K. DRIDI, AND J. HESTHAVEN, *Convergent Cartesian grid methods for Maxwell's equations in complex geometries*, Journal of Computational Physics, 170 (2001), pp. 39–80.

[10] T. A. DRISCOLL AND B. FORNBERG, *A block pseudospectral method for Maxwell's equations I: One-dimensional case*, Journal of Computational Physics, 140 (1998), pp. 47–65.

[11] ———, *Block pseudospectral methods for Maxwell's equations II: Two-dimensional, discontinuous coefficients case*, SIAM J. Sci. Comput., 21 (1999), pp. 1146–1167.

[12] B. FORNBERG, *A Practical Guide to Pseudospectral Methods*, Cambridge University Press, 1996.

[13] S. D. GEDNEY, F. S. LANSING, AND D. L. RASCOE, *Full wave analysis of microwave monolithic circuit devices using a generalized Yee-algorithm based on an unstructured grid*, IEEE Transactions on Microwave Theory and techniques, 44 (1996), pp. 1393–1400.

[14] B. GUSTAFSSON, H.-O. KREISS, AND J. OLIGER, *Time Dependent Problems and Difference Methods*, John Wiley and Sons Inc., 1995.

[15] B. GUSTAFSSON AND E. MOSSBERG, *Time compact high order difference methods for wave propagation problems*, SIAM J. Sci. Comput., 26 (2004), pp. 259–271.

[16] B. GUSTAFSSON AND P. WALHUND, *Time compact high order difference methods for wave propagation in discontinuous media*, SIAM J. Sci. Comput., 26 (2004), pp. 272–293.

[17] C. HAZARD, *Numerical simulation of corner singularities: A paradox in Maxwell-like problems*, C.R. Mecanique, 330 (2002), pp. 57–68.

[18] C. HAZARD AND S. LOHRENGEL, *A singular field method for Maxwell's equations: Numerical aspects for 2D magnetostatic*, SIAM J. Numer. Anal., 40 (2002), pp. 1021–1040.

[19] W. HENSHAW, *Mappings for Overture, a description of the Mapping class and documentation for many useful Mappings*, Research Report UCRL-MA-132239, Lawrence Livermore National Laboratory, 1998.

[20] W. HENSHAW, H.-O. KREISS, AND L. REYNA, *A fourth-order accurate difference approximation for the incompressible Navier-Stokes equations*, Comput. Fluids, 23 (1994), pp. 575–593.

[21] W. D. HENSHAW, *On multigrid for overlapping grids*, SIAM Journal of Scientific Computing, 26 (2005), pp. 1547–1572.

[22] W. D. HENSHAW AND D. W. SCHWENDEMAN, *An adaptive numerical scheme for high-speed reactive flow on overlapping grids*, J. Comput. Phys., 191 (2003), pp. 420–447.

[23] J. HESTHAVEN AND T. WARBURTON, *Nodal high-order methods on unstructured grids, I. time-*

domain solution of Maxwell's equations, J. Comp. Physics, 181 (2002), pp. 186–221.

[24] R. HOLLAND, *Finite difference solution of Maxwell's equations in generalized nonorthogonal coordinates*, IEEE Transactions on Nuclear Science, 30 (1983), pp. 4589–4591.

[25] J. JIN, *The Finite Element Method in Electromagnetics*, John Wiley and Sons, New York, 1993.

[26] H. JURGENS AND D. ZINGG, *Numerical solution of the time-domain Maxwell equations using high-accuracy finite-difference methods*, SIAM J. Sci. Comput., 22 (2000), pp. 1675–1696.

[27] H.-O. KREISS AND N. A. PETERSSON, *A second order accurate embedded boundary method for the wave equation with Dirichlet data*, Research Report UCRL-JRNL-202686, Lawrence Livermore National Laboratory, 2004. (to appear SIAM J. Sci. Comput.).

[28] H.-O. KREISS, N. A. PETERSSON, AND J. YSTRÖM, *Difference approximations for the second order wave equation*, SIAM J. Numer. Anal., 40 (2002), pp. 1940–1967.

[29] J. LAMBERT, *Computational Methods in Ordinary Differential Equations*, Cambridge University Press, New York, 1973.

[30] J. LEE, R. PALENDECH, AND R. MITTRA, *Modeling three-dimensional discontinuities in waveguides using nonorthogonal FDTD algorithm*, IEEE Trans. Microwave Theory and Techniques, 40 (1992), pp. 346–352.

[31] R. LEHOUCQ, D. SORENSEN, AND C. YANG, *ARPACK User's Guide*, SIAM, Philadelphia, 1998.

[32] N. K. MADSEN, *Divergence preserving discrete surface integral method for Maxwell's curl equations using non-orthognal unstructured grids*, J. Comput. Phys., 119 (1995), pp. 34–45.

[33] J. NÉDÉLEC, *Mixed finite elements in R^3*, Numer. Math., 35 (1980), pp. 315–341.

[34] D. QUINLAN, *A++/P++ class libraries*, Research Report LA-UR-95-3273, Los Alamos National Laboratory, 1995.

[35] L. G. M. REYNA, *Part III. On Composite Meshes*, PhD thesis, Dept. of Applied Mathematics, California Institute of Technology, 1982.

[36] P. ROACHE, *Code verification by the method of manufactured solutions*, ASME J. of Fluids Engineering, 124 (2002), pp. 4–10.

[37] G. RODRIGUE AND D. WHITE, *A vector finite element time-domian method for solving Maxwell's equations on unstructured hexahedral grids*, SIAM J. Sci. Comput., 23 (2001), pp. 683–706.

[38] T. RYLANDER AND A. BONDESON, *Application of stable FEM-FDTD hybrid to scattering problems*, IEEE Transactions on Antennas and Propogation, 50 (2002), pp. 141–144.

[39] G. R. SHUBIN AND J. B. BELL, *A modified equation approach to constructing fourth order schemes for acoustic wave propagation*, SIAM J. Sci. Stat. Comput., 8 (1987), pp. 135–151.

[40] A. SUSSMAN, G. AGRAWAL, AND J. SALTZ, *A manual for the Multiblock PARTI runtime primitives, revision 4.1*, Technical Report CS-TR-3070.1, University of Maryland, Department of Computer Science, 1993.

[41] A. TAFLOVE AND S. C. HAGNESS, *Computational Electrodynamics: The Finite-Difference Time-Domain Method*, Artech House, 2000.

[42] H. VAN DE HULST, *Light Scattering by Small Particles*, Dover Publications, Inc., 1957.

[43] B. YANG, D. GOTTLIEB, AND J. HESTHAVEN, *Spectral simulations of electromagnetic wave scattering*, J. Comp. Physics, 134 (1997), pp. 216–230.

[44] K. YEE, *Numerical solution of initial boundary value problems involving Maxwell's equations in isotropic media*, IEEE Transactions on Antennas and Propogation, 14 (1966), pp. 302–307.

[45] K. S. YEE, J. S. CHEN, AND A. H. CHANG, *Conformal finite-difference time-domain (FDTD) with overlapping grids*, IEEE Transactions on Antennas and Propogation, 40 (1992), pp. 1068–1075.